MIT Open Access Articles

Electrode–Electrolyte Interface in Li-Ion Batteries: Current Understanding and New Insights

TITLE: The Electrode-Electrolyte Interface in Li-ion Batteries: Current Understanding and New Insights

AUTHOR NAMES: *Magali Gauthier,*[†‡♯] *Thomas J. Carney,*[‡§♯] *Alexis Grimaud,*[†‡▽∥♯] *Livia Giordano,*[†‡♮] *Nir Pour,*[‡†] *Hao-Hsun Chang,*[†‡] *David P. Fenning,*[‡/◊] *Simon F. Lux,*[¶] *Odysseas Paschos,*[⊥] *Christoph Bauer,*[⊥] *Filippo Maglia,*[⊥] *Saskia Lupart,*[⊥] *Peter Lamp,*[⊥] *Yang Shao-Horn*[†‡§/]*

AUTHOR ADDRESS: †Research Laboratory of Electronics, ‡Electrochemical Energy Laboratory, §Department of Materials Science & Engineering, and │Department of Mechanical Engineering, Massachusetts Institute of Technology, 77 Massachusetts Avenue, Cambridge, Massachusetts 02139, United States

♮Dipartimento di Scienza dei Materiali, Università di Milano-Bicocca, Via R. Cozzi 55, 20125 Milan, Italy

¶BMW Group Technology Office USA, 2606 Bayshore Parkway, Mountain View, California 94043, United States

⊥BMW Group, Petuelring 130, 80788 München, Germany

AUTHOR INFORMATION

Corresponding Author

* To whom correspondence should be addressed: shaohorn@mit.edu

\# M.G., T.J.C., and A.G. contributed equally to this work

Present Addresses

A.G. current addresses: ▽FRE 3677 "Chimie du Solide et Energie," Collège de France, 75231

Paris Cedex 05, France.‖Réseau sur le Stockage Electrochimique de l'Energie (RS2E), FR

CNRS 3459, 80039 Amiens Cedex, France.

D.P.F. current address : ◊Department of Nanoengineering, UC San Diego, La Jolla, CA 92093

ABSTRACT. Understanding reactions at the electrode/electrolyte interface (EEI) is essential to developing strategies to enhance cycle life and safety of lithium batteries. Despite research in the past four decades, there is still limited understanding by what means different components are formed at the EEI and how they influence EEI layer properties. We review findings used to establish the well-known mosaic structure model for the EEI (often referred to as solid electrolyte interphase or SEI) on negative electrodes including lithium, graphite, tin and silicon. Much less understanding exists for EEI layers for positive electrodes. High-capacity Li-rich layered oxides $yLi_{2-x}MnO_3 \bullet (1-y)Li_{1-x}MO_2$, which can generate highly reactive species toward the electrolyte via oxygen anion redox, highlight the critical need to understand reactions with the electrolyte and EEI layers for advanced positive electrodes. Recent advances in *in situ* characterization of well-defined electrode surfaces can provide mechanistic insights and strategies to tailor EEI layer composition and properties.

TOC GRAPHIC
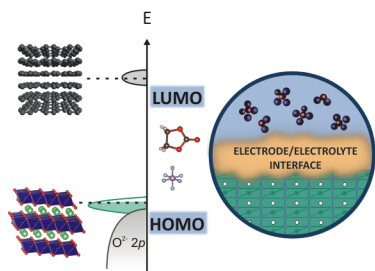
The use of lithium-ion (Li-ion) batteries to power hybrid, plug-in hybrid and electrical vehicles in recent years calls for greater battery cycle life and safety characteristics than their applications in electronic devices. Li-ion batteries operate by shuttling Li^+ and electrons between negative and positive electrode host structures,[1–5] which are separated by a separator filled with an aprotic electrolyte. Negative electrodes operate at potentials close to 0 V_{Li} (Li^+/Li) storing lithium near the neutral valence state[4,6] while positive electrodes normally store lithium ions at potentials greater than 3 V_{Li}.[5,7–10] Aprotic electrolytes can be thermodynamically unstable against reduction at negative electrodes[11–15] and against oxidation at the positive electrodes.[16–22] The formation of a stable electrode-electrolyte interface (EEI) layer, conductive to Li^+ but electronically insulating, is critical to ensure high coulombic and voltage efficiency,[23] cycle life[23,24] and safety[24,25] over the course of battery lifetime for vehicle applications.[25] Understanding electrochemical and chemical reactions between the electrode and the electrolyte, which influence the composition, microstructure and properties of EEI layers formed, is crucial in developing stable and efficient Li-ion batteries.

Carbonate-based electrolytes commonly used in Li-ion batteries are reduced on negative electrodes such as graphite to form the well-known solid electrolyte interphase (SEI).[26–32] Li^+-conducting and electronically insulating SEI[26,31] can prevent continuous electrolyte reduction and lithium consumption during cycling.[33–36] However, the formation of non-uniform SEI can result in non-uniform lithium deposition and formation of lithium dendrites,[37–39] which can lead to battery internal short and failure.[37] The electrolyte oxidation on the positive electrodes and the composition and properties of the EEI layer, if any, are less understood than the SEI on negative electrodes.[40–43] Recent advances in high-capacity positive materials, which can generate highly reactive oxygen species,[44–49] highlight the need to study EEI layers on their surfaces. Such

4

understanding is key to mitigate the electrolyte reactivity with positive electrodes, which can affect battery life and safety as exothermic reactions of positive electrodes with flammable electrolytes lead to substantial heat generation, triggering thermal runaway.[50–53]

Progress in understanding the EEI layers on Li-ion negative and positive electrodes has been achieved using techniques such as X-Ray Photoelectron Spectroscopy (XPS),[40,54–63] Fourier Transform Infrared Spectroscopy (FTIR),[11,29,41,54,64,65] X-Ray Diffraction (XRD),[54,66] Atomic Force Microscopy (AFM)[67–69] and Scanning Tunneling Microscopy (STM) [70–72] However, while significant work[26–28,32,40,41,46,56–58,62,63,65,69,73–83] has studied the EEI layer, much remains to be understood at the fundamental level. Despite considerable research in the past few decades, the SEI is still a puzzle to be solve due to a lack of questioning of the past results and to an excessive confidence in the miraculous properties of the SEI.[77] There is still limited understanding on what EEI layers consist of, by what mechanisms they are formed and how they influence EEI properties and battery performance.

In this perspective paper, we first review and discuss thermodynamic considerations of electrolyte reduction and oxidation on negative and positive electrodes. Second, we discuss the historical evolution of the concept of the SEI composition and structure on lithium and graphite, which depends on the salt and solvent used in the electrolyte and on the surface termination of the electrode. Third, we compare SEI compositions found on lithium and graphite with those reported for alloyed negative electrodes such as Sn and Si. Fourth, we summarize the EEI layer models reported for oxides of positive electrodes, where the nucleophilicity of oxide surfaces is correlated with EEI layer composition and impedance. In addition, there is a critical need to understand the electrolyte oxidation with high-capacity oxide electrodes that release highly reactive oxygen species, where much learning can derive from knowledge on electrolyte

instability developed in the Li-O$_2$ chemistry.[84–91] Lastly, we will discuss opportunities and techniques that can be used to gain mechanistic insights underlying EEI layer formation and composition and how its properties contribute to battery performance.

Thermodynamic considerations of electrolyte instability. The difference between the Fermi level of the electrode and the highest occupied molecular orbital (HOMO) or the lowest unoccupied molecular orbital (LUMO) levels of the electrolyte governs the thermodynamic stability of the electrolyte on the electrode and the driving force to form the EEI layer.[2,92] A negative electrode with a Fermi level higher in energy than the LUMO of the electrolyte will have a driving force to reduce the electrolyte (Figure 1b).[2] On the positive side, there will be a driving force for electrolyte oxidation if the Fermi level of the electrode is lower in energy than the HOMO of the electrolyte (Figure 1b).[2] Below we review and align electron energy levels associated with lithium insertion in electrodes with estimated LUMO and HOMO of electrolytes to discuss the thermodynamic driving force for EEI layer formation associated with electrolyte instability on the electrode surface.

Lithium storage electrode potentials. The electrochemical potential of an electrode for lithium storage (the energy level for electron transfer to and from the material, or redox electron energy) corresponds to the average electron energy level at the top of the itinerant or valence band. The difference between the electrochemical potentials of the negative and positive electrodes defines the thermodynamic cell voltage. Lithium and graphite, the most common negative electrodes storing lithium at 0 and ~0.1 V_{Li},[4,93] respectively, have Fermi levels that lie in an itinerant band[2] above the estimated LUMO levels of electrolytes, as shown in Figure 1a. Similarly, high-capacity alloy electrodes such as Sn[94] and Si[95] storing lithium in the range of ~ 0-1 V_{Li}, also have

Fermi levels above the estimated LUMO levels of aprotic electrolytes. Therefore, there is a thermodynamic driving force for electrochemical reduction of electrolytes at the surface of these negative electrodes. Employing surface films at the EEI (also called SEI), which are stable, electronically insulating and lithium ion conducting, can passivate the electrode surface and prevent direct contact of the aprotic electrolyte to the electrode surface.
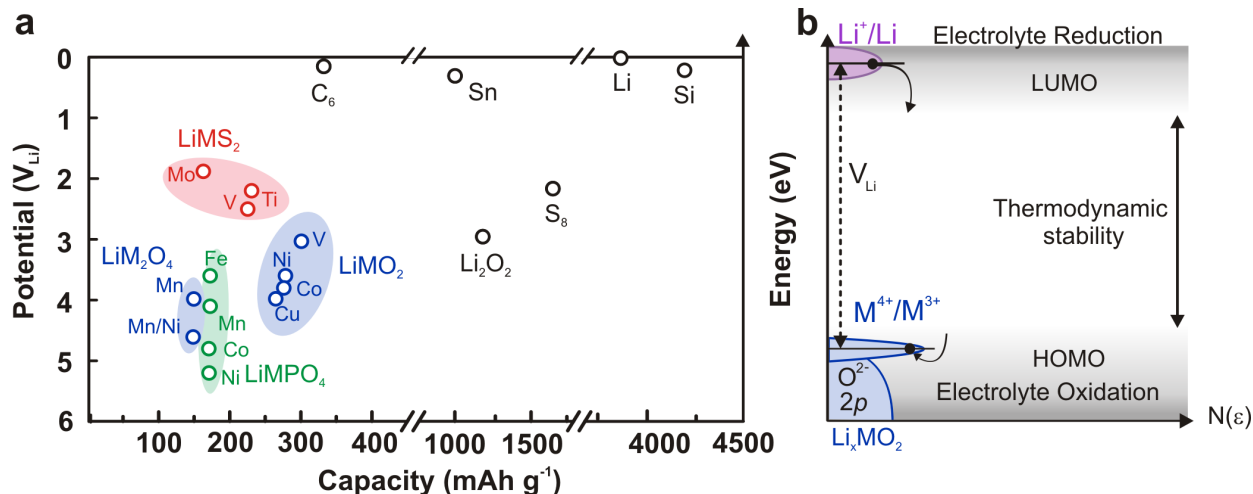

Figure 1. a) Potentials and expected capacities based on full extraction of selected lithium storage materials for Li-ion batteries (details on the potentials reported from previous work and calculations of capacities can be found in the SI).[4,5,10,93–107] Expected capacities of selected intercalation compounds (based on full lithium extraction) can vary from low values around 150-200 mAh g^{-1} to 350 mAh g^{-1} for positive and negative electrodes respectively (details in SI). Lithiation of Sn[94] and Si[95] alloys (voltage range 0.1-1 V$_{Li}$), and new chemistries such as Li-O$_2$ (Li$_2$O$_2$, 2.96 V$_{Li}$)[106] and Li-S (S$_8$, 2.2 V$_{Li}$)[107] (see details in SI) offer much higher capacity. b) The difference between electron energy levels associated with electrode redox and the HOMO/LUMO levels of the electrolyte governs the thermodynamic stability of electrode/electrolyte at the EEI and driving force to form the EEI layers.[2] Shaded areas represent the potential ranges for electrolyte reduction and oxidation.

Lithium transition metal compounds such as oxides, sulfides and phosphates have electrochemical potentials (Figures 1a,b) that are lower than the LUMO level of aprotic electrolytes. Thus they are stable against thermodynamic reduction of electrolytes. Their electrochemical potentials are determined largely by the redox energy of transition metal ions, which can be tuned to a large extent by transition metal d states (including d electron number and oxidation state), and to a small extent by the covalency of metal-anion bonds (or the mixing of transition metal d states with the anion p states).[2,108,109] For example, going from the left to the right for first-row transition metal ions, the transition metal d states are lowered, resulting in higher lithium intercalation voltages such as in $LiMPO_4$ (M = Fe, Mn, Co and Ni) (Figure 1a). On the other hand, utilizing an inductive effect associated with M-O-P instead of M-O frameworks like in $LiMO_2$, the redox energy of transition metal ions can be further lowered (further increasing lithium intercalation potentials, Figure 1a).[10,101–104] Some high-voltage lithium storage materials such as $Li_{1-x}CoO_2$ (x < 0.7 above 4.5 V_{Li}),[110] $Li_{1-x}Mn_{1.5}Ni_{0.5}O_4$ (Ni^{4+}/Ni^{2+} at 4.7 V_{Li})[105] and $Li_{1-x}NiPO_4$ ($Ni^{2+/3+}$ at 5.2 V_{Li})[104] have very low redox energy levels, approaching the HOMO levels of aprotic electrolytes, as shown in Figure 1a, which can result in a thermodynamic driving force for electrolyte oxidation on the electrode and for surface films formation. Furthermore, recent high-capacity layered electrodes $yLi_{2-x}MnO_3 \bullet (1-y)Li_{1-x}MO_2$ (M = Ni, Co, Mn), referred as composites[111–113] or solid solutions (or Li-rich $Li_{1+y}M_{1-y}O_2$),[44,114,115] and Li_2MO_3 (M= Ru, Mn, Ti, Sn)[48,49,116,117] employ oxide anion redox for lithium storage in addition to transition metal redox (delivering reversible capacities greater than 230 mAh g^{-1}, compared to ~ 140 mAh g^{-1} for the practical capacity of $LiCoO_2$ (see SI)),[44,48,49,111–114,116,117] where transition metal d states fall below the oxygen anion p band.[2,118,119] Anionic redox in these oxides can trigger the formation of highly reactive species such as peroxide ions O_2^{2-},[2,118,119] molecular

8

oxygen,[2,119–121] and superoxide (O_2^- formed upon reduction of O_2 at voltages below ~ 3 V_{Li}),[106,122] which can chemically react with aprotic electrolytes[84–88] to form surface films.

Estimated LUMO/HOMO levels of electrolytes. The LUMO and HOMO levels of the electrolyte can be estimated from the first adiabatic electron transfer to and from the bulk of the electrolyte, respectively (Figures 2a and 2b).[14–16,18,22,123,124] Solvent molecules and Li^+-solvent or anion-solvent complexes are used to describe the reduction and oxidation of pure solvent and solvated salts, respectively.[14–16,18,22,123,124] The reduction potentials (associated with the LUMO levels) were computed using hybrid functional DFT calculations in Polarizable Continuum Model (PCM), as detailed in the SI and agree with previous studies.[14,15,123] Pure carbonate solvents used commonly in Li-ion batteries such as ethylene carbonate (EC), propylene carbonate (PC) and dimethyl carbonate (DMC) have computed LUMO levels close to the Li^+/Li couple,[14,15,123] as shown in Figure 2a. No significant difference is noted for the LUMO levels of pure PC, EC and DMC, indicating that changing the carbon chain attached to the carbonate group does not affect the LUMO level since the electron transferred is localized at the carbonate group, as shown in Figure 2b. When lithium ions are included in the calculations, the computed LUMO levels of these electrolytes decrease by ~0.5 eV relative to pure solvents, rendering these electrolytes thermodynamically unstable against reduction on lithium and graphite, as depicted in Figure 2a. This decrease in the thermodynamic stability against electrochemical reduction can be explained by lithium ion interaction with the extra electron localized at the carbon center of the carbonate group of the solvent molecule.[14,15,123] In addition to the role of lithium ions on the LUMO level of electrolytes, the influence of salt anions such as PF_6^-, ClO_4^- and BF_4^- should be considered, which will require further computational studies. This consideration is particularly important as salt anions have been experimentally determined to play an important role in the

9

stability of electrolytes on the negative electrode[56,125–127] and the impedance of SEI films (Figures 2c,d).[29,73,128] Species with elements unique to salt anions such as lithium fluoride (LiF) have been detected in the SEI at the negative electrode surface,[62,73,129] which will be discussed in detail below.
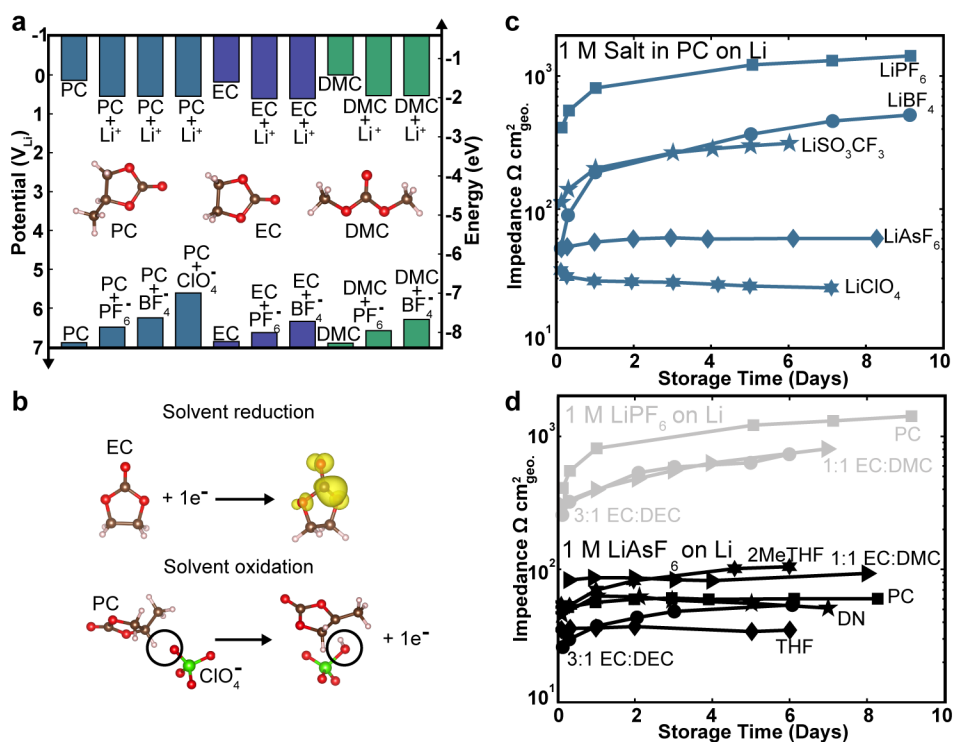

Figure 2. a) Computed reduction and oxidation[16,18,124] energy levels of common Li-ion battery solvents and solvated salts. b) Reactions used to calculate the reduction and oxidation potentials and the energy levels on the absolute scale. The potential values are converted from the absolute potential scale to the Li$^+$/Li potential scale by subtracting 1.4 V.[17] The oxidation potentials of the pure salt anions are 8.58 V$_{Li}$ for PF$_6^-$, 6.11 V$_{Li}$ for ClO$_4^-$ and 8.35 V$_{Li}$ for BF$_4^-$.[17] c) Impedance of surface films formed on lithium foil upon storage for various 1 M salt-based electrolytes in PC.[73] d) Impedance of surface film on lithium foil upon storage for 1 M LiAsF$_6$ and 1M LiPF$_6$ in various solvents (see SI for details).[29,128] The impedance values include all the impedance

contributions of the electrode. However, as the charge transfer resistance is considered negligible for lithium foil, the total impedance can be attributed largely to the interface film resistance (See SI for details of data extraction).

The computed HOMO levels of pure carbonate solvents (data taken from the literature[16,18,124] as detailed in the SI) are below the redox energy of positive electrode materials (Figure 1a), as the corresponding oxidation potential is close to 7 V_{Li} (Figure 2a).[18] When a salt anion is added to the solvent, the computed HOMO levels of the electrolytes are increased by up to ~1.5 eV (potential about 5.5 V_{Li}) (Figure 2a), making the electrolytes thermodynamically less stable against electrochemical oxidation, where a proton transfer between the solvent and the salt anion follows the oxidation of the electrolyte (Figure 2b).[16,124] The thermodynamic stability trend of the electrolytes examined decreases in order from PF_6^-, BF_4^- and ClO_4^-, with electrolyte solvents coupled with PF_6^- being the most thermodynamically stable against oxidation, as shown in Figure 2a.

Although DFT calculations predict the electrolyte solvents to be thermodynamically stable against oxidation at potentials below ~ 5.5 V_{Li} (Figure 2a), experimental studies show that carbonate-based electrolytes can be oxidized electrochemically in the range 4.5-6.5 V_{Li}.[19–21] This discrepancy can result from the presence of impurities, variations in determining experimental oxidation/reduction potentials,[18] different catalytic activities of the electrodes used for the measurement[124] and/or insufficient accuracy in the current DFT calculations. Indeed, while the computed data reported in Figure 2a indicate clear trends, taking the computed HOMO/LUMO of solvent molecules as a measure of the electrochemical stability window neglects the interactions between the solvent and the electrode surface which can change the solvent energy

levels[22] and does not take into account the difference between the initial and transition states of electron transfer,[130] which ultimately governs the kinetics of electrolyte decomposition.[74]
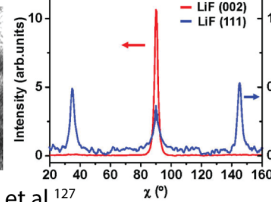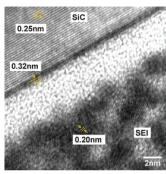
In addition to electrochemical reduction or oxidation of the electrolyte described in Figures 2a and 2b, electrolytes can decompose by chemical reactions, which can compete with or follow these electrochemical reactions, influencing components formed in the EEI layer.[131] In the following sections, we will highlight selected negative and positive electrodes to explore how electrochemical and chemical reactions contribute to the composition and structure of the EEI layer and how the electrode composition and termination can influence them.

Towards understanding of the EEI layer on negative electrodes. In this section, we will first introduce the historical evolution of the concept of the EEI layer composition and structure on lithium, graphite and alloys electrodes, which depends on the salt and solvent used in the electrolyte and on the surface termination of the electrode. An ideal SEI on the negative electrode should allow lithium diffusion for reversible insertion in the material while preventing further reduction of electrolyte at the surface. Although the well-known mosaic model of the SEI on lithium and graphite described below is well accepted in the community, it has not been fully experimentally established and enough challenged and fundamental understanding is still needed to definitively determine what and how species are formed on the surface, and how applied potential and cycling influence it. The development of synchrotron[63,127,132] and *in situ* techniques[69,133,134] should help find the missing pieces of the SEI puzzle.

SEI on lithium. Our current understanding of the SEI comes from the progressive build-up of knowledge in the past four decades brought by a large body of work (Figure 3). Peled[26] first introduced the concept of a single layer SEI on alkali or alkaline earth metals formed
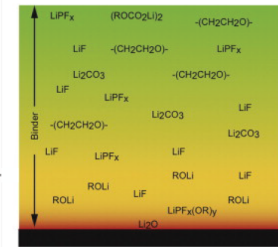
12

instantaneously upon contact with electrolyte (1979, Figure 3), whose electronic and ionic properties are similar to a solid electrolyte, specifically electronically insulating but ion conducting. Subsequently, he proposed a double layer SEI structure with a thin compact layer close to the electrode and a thick porous secondary layer closer to the electrolyte (1983).[135,136] These initial models from Peled have no compositional information for the SEI formed. Nazri and Muller[54,66] first showed the presence of Li_2CO_3 and oligomers (or polymers) in SEI on lithium surfaces using XPS, FTIR and *in situ* XRD.[54,66] Later Aurbach et al.[137] revealed through FTIR/XPS that lithium alkyl carbonates (dicarbonates or semicarbonates) instead of Li_2CO_3 are the main SEI components, resulting from carbonate solvent decomposition, even if the presence of traces of Li_2CO_3 cannot be excluded (Figure 3).[137] Moreover, Kanamura et al.[56,57] reported by XPS that the compact layer near the lithium surface consists of LiF and Li_2O while the porous layer above contains LiF and organic compounds (Figure 3). Peled et al. summarized previous findings and reported the first mosaic structure of the SEI[27,31] (Figure 3), which is used widely today. The SEI mosaic structure consists of multiple inorganic and organic products from electrolyte decomposition (Figure 3, Table S3): near the lithium surface, compact layers are formed of inorganic species like Li_2O, Li_2CO_3, and LiF, thermodynamically stable against lithium;[27,29,31,56] near the electrolyte, the layers consist mainly of oligomer species (polyolefins, Figure 3) and semicarbonates.[27,29,31,56]
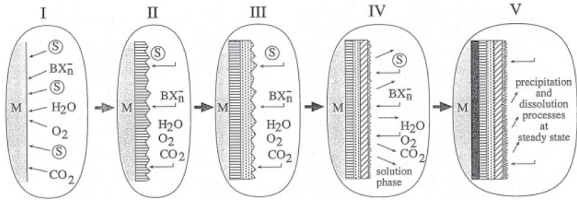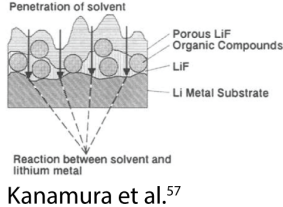
2012

In situ X-ray scattering

SiC
0.25nm
0.32nm
0.20nm
SEI
2nm

LiF (002)
LiF (111)

Intensity (arb.units)

χ (°)

Chattopadhyay et al.[127]

2013

LiPF$_x$ (ROCO$_2$Li)$_2$ -(CH$_2$CH$_2$O)-
LiF -(CH$_2$CH$_2$O)- LiPF$_x$
Li$_2$CO$_3$ -(CH$_2$CH$_2$O)-
LiF LiPF$_x$
Binder -(CH$_2$CH$_2$O)- Li$_2$CO$_3$ LiF
LiPF$_x$ LiF Li$_2$CO$_3$
LiF ROLi LiF
ROLi LiF ROLi
LiPF$_x$(OR)$_y$
Li$_2$O

Malmgren et al.[63]

2010

2006

Porous organic layer
Inorganic layer
LiF crystals
LiF
Graphite

Edström et al.[62]

1999

I II III IV V

S BX$_n^-$ H$_2$O O$_2$ S CO$_2$

M BX$_n^-$ M BX$_n^-$ M BX$_n^-$ M

precipitation and dissolution processes at steady state

solution phase

Aurbach et al.[28]

2000

1997

Li$_2$O
LiF
Polyolephines
Li$_2$CO$_3$
Li$_2$O LiF
LiF Li$_2$O
LiF Li$_2$CO$_3$
semi-carbonates

Li or Carbon

Peled et al.[27]

1995

Penetration of solvent
Porous LiF Organic Compounds
LiF
Li Metal Substrate
Reaction between solvent and lithium metal

Kanamura et al.[57]

1995

graphene-layer

RX (donor solvent)
R (decomposed solvent)
Li$^+$
LiX

Besenhard et al.[139]

1994

The multi layer model and related equivalent circuit analog

low capacitance high capacitance

Li Side layer a layer b layer c layer d interface ? solution res. soln. side

the compact interphase the porous interphase

high frequencies → low frequencies

Aurbach et al.[73]

1983

Li

Secondary Porous layer Solution

Electrolyte concentration (M)

SEI

Distance from SEI (μ)

Peled[135]

1990

1987

Lithium alkyl carbonates as main SEI component on Li (FTIR/XPS), Aurbach et al.[137]

1985

Li$_2$CO$_3$ and polymers on lithium (FTIR/XPS/XRD) Nazri and Muller[54,66]

1980

1979

$M^+_{M/SE} + e\ (M) \leftrightarrows M^o_M$

M SE

Peled[26]

1970

1977

Microscopic observation of surface film on lithium soaked in electrolyte, Dey et al.[138]
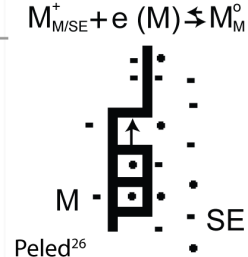
Figure 3. Evolution of knowledge and models of the SEI on negative electrodes in the past four decades. First attempts to characterize the formation of surface species on lithium were made in the 70-80s by Dey et al.,[138] Nazri and Muller[54,66] and Aurbach et al.[137] Meanwhile, Peled[26] introduced the concept of the SEI in 1979 and he further refined the model (1983,[135] 1997)[27] based on Electrochemical Impedance Spectroscopy (EIS) data and results by Aurbach et al.[73] (1994) and Kanamura et al.[57] (1995). On another hand, Besenhard et al.[139] proposed a 3D formation model of the SEI where solvent molecules cointercalate in the graphite layers to further decompose and form a SEI. Since 1997, researchers aim to provide unambiguous evidence for the mosaic model of the SEI on lithium and graphite electrodes (Aurbach 1999,[28] Edström 2006)[62] using for example synchrotron (Malmgren et al.,[63] 2013) and *in situ* techniques (Chattopadhyay et al.,[127] 2012). Reproduced with permission from ref 26. Copyright 1979, The Electrochemical Society. Reprinted with permission from ref 57. Copyright 1995, The Electrochemical Society. Reprinted with permission from ref 27. Copyright 1997, The Electrochemical Society. Reprinted from refs 28,62,63,73,135,139 with permission from Elsevier. Reprinted with permission from ref 127.

The SEI impedance on lithium can be influenced greatly by the salt in the electrolyte through changes in the SEI composition or structure. Aurbach et al.[29,73,128] showed that changing the salt anion increases the impedance in the order $PF_6^- > BF_4^- \approx SO_3CF_3^- > AsF_6^- > ClO_4^-$, with an increase of the total impedance by almost two orders of magnitude from ClO_4^- to PF_6^- (Figure 2c). In addition, the impedance of lithium soaked with $LiAsF_6$ and $LiClO_4$ stabilized more rapidly than $LiPF_6$ and $LiBF_4$ (Figure 2c),[73] suggesting faster formation of electronically insulating SEI with AsF_6^- and ClO_4^- anions. These results indicated that the decomposition of

anions, which produces inorganic components such as LiF (for $LiPF_6$, $LiAsF_6$ and $LiBF_4$) or LiCl (for $LiClO_4$) in the SEI on lithium, strongly influences the impedance.[73] The higher impedance observed for $LiPF_6$ and $LiBF_4$ is attributed to the higher concentration of highly resistive LiF[128] in the SEI, supposedly produced by the gradual decomposition of carbonates by traces HF from the salt (Table S3).[29,73,128] Varying the nature of the solvent does not modify significantly the impedance (Figure 2d) even though it affects remarkably the composition of the SEI on lithium. In ether solvents (tetrahydrofuran, dimethylether), the major SEI products are lithium alkoxides (ROLi) whereas lithium carboxylates (RCO_2Li) are the main SEI species in ester solvents (methylformate, γ-butyrolactone) (Table S3).[140,141] In the case of the popular carbonate solvents, Li_2CO_3, Li dicarbonates (($ROCO_2Li)_2$) and semicarbonates ($ROCO_2Li$) predominate in the SEI (Table S3).[29,74,137,142,143] The composition of the electrolyte plays also an indirect role on the SEI by affecting the formation of dendrite during cycling.[64,144,145] Dendrite formation has for instance been mitigated using electrolyte solutions based on 1,3-dioxolane stabilized with ternary amines.[145] The use of highly concentrated electrolytes based on ether[146,147] or amides[148] allow also for the formation of a stable SEI and lead to smoother and more uniform lithium deposition. The choice of the solvent is thus critical for the formation of a stable SEI leading to homogeneous deposition and stripping of lithium, which finally determines the coulombic efficiency of the cell.

SEI on carbonaceous surfaces. Current understanding of SEI on carbonaceous surfaces adopts a similar composition and mosaic structure to that on lithium foil (Figure 3). However, in contrast to lithium where the SEI is formed by simple contact with the electrolyte, the SEI develops on graphite/carbons when the electrode potential drops below 1 V_{Li}. Dahn et al.[30] first

showed that lithium ions can be intercalated reversibly in graphitic carbon in liquid electrolyte using ethylene carbonate (EC), which is attributed to the formation of an electronically insulating SEI that prevents both further decomposition of the electrolyte and co-intercalation of EC into the graphite, in contrast to irreversible lithium intercalation associated with graphite exfoliation in PC. It is still not completely understood why such as small difference between PC and EC (one methyl group) can generate such different properties and composition of the SEI.[77] The mosaic model of SEI on graphite in presence of EC, similar to that on lithium metal, was supported mainly by Peled et al. using XPS,[55,76,149] Aurbach et al. using FTIR,[29,150–155] and Ogumi et al. using AFM[67,68,156] and STM.[71,72] Significantly, EC forms a stable SEI composed mainly of lithium ethylene dicarbonate $(CH_2OCO_2Li)_2$.[29,143,150–155]
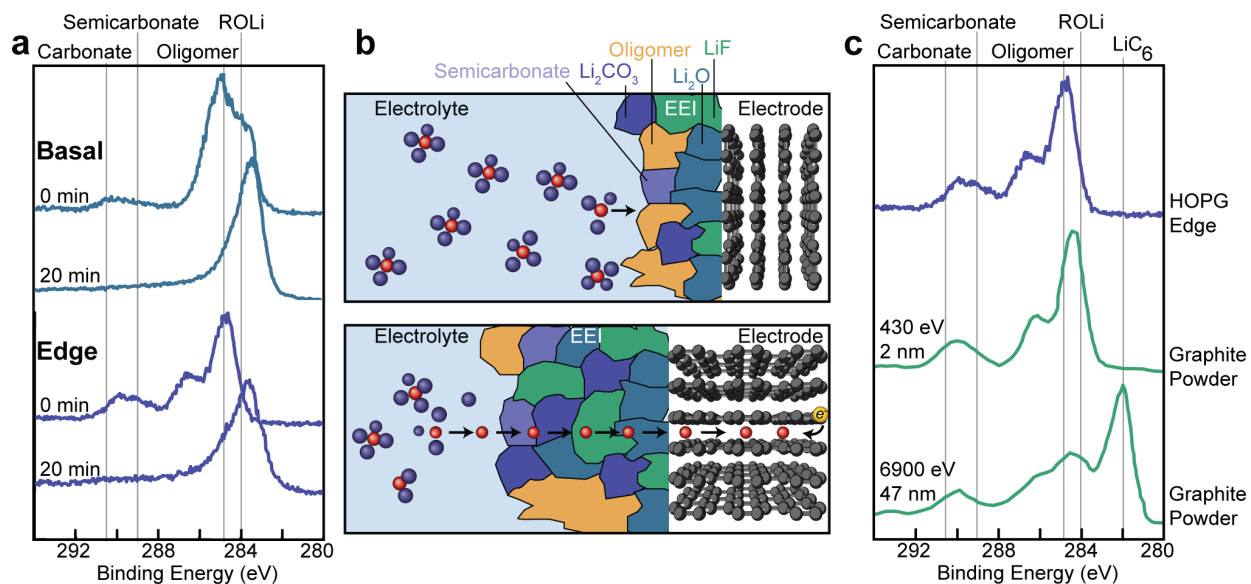
Figure 4. a) XPS C1s data from HOPG basal and edge electrodes cycled in 1 M $LiAsF_6$ in 1:2 EC: diethylene carbonate (DEC), showing mostly the presence of oligomers on the basal plane and of a mix of carbonates, semicarbonates and oligomers on the edge. The electrodes were discharged to 0.2 V_{Li} and then charged to 2.5 V_{Li}. Data are shown for no Ar sputtering, 0 min, and after 20 min of Ar sputtering.[129] b) Schematic of the SEI on basal (top) and edge (bottom)

planes. The SEI on the basal plane consists mostly of solvent decomposition products (organic) while the edge plane is composed mainly of salt decomposition products (inorganic).[55,76,129,149] c) XPS of a composite graphite electrode based of 85 wt% graphite powder, 5% carbon, and 10% binder (vinylidene fluoride trifluoroethylene co-polymer, dissolved in NMP) in 1 M LiPF$_6$ EC:DEC after 3.5 cycles, final state is lithiated. The different depths are obtained by tuning the incident photon energy.[63] The graphite electrode SEI is similar in composition to the SEI of the HOPG edge electrode (0 min).[129]

Studying SEI on model surfaces such as the basal and edge surfaces of HOPG[55,129,149] reveals that basal and edge planes result in different SEI compositions and thicknesses (Figures 4a and 4b). On the basal plane, the SEI after one cycle (one discharge to 0.2 V$_{Li}$ and one charge to 2.5 V$_{Li}$) consists of organic species from solvent reduction, while on edge planes the SEI is mostly inorganic due to salt reduction.[55,129,149] Comparing C1s XPS spectra of edge and basal planes after cycling, the outermost surface of the basal SEI (Figure 4a, no Ar sputtering, 0 min) is composed mainly of oligomers ($\sim$ 65%) and a small amount of carbonates and semicarbonates ($\sim$ 13%), while the edge SEI consists of both carbonates and semicarbonates ($\sim$ 32%), and oligomers (32%).[129] SEI depth profiling from Ar sputtering reveals that SEI products shift from organic products to inorganic species like Li$_2$O, As, Li$_2$CO$_3$ and ROLi,[129] moving towards the basal or edge surface, similar to what has been demonstrated for lithium.[27,29,31,56] This finding is supported by recent *in situ* AFM studies on HOPG, showing a bilayer structure of the SEI with an upper SEI soft and organic and a dense and salt-based layer close to the electrode.[69] Closer to the electrode surface (after Ar sputtering for 20 min), the LiF atomic concentration in the edge SEI rises to ~70% compared to 20% for basal SEI, confirming the predominance of salt decomposition on the edge.[129] Moreover, XPS studies show that SEI on the basal plane (~7 nm)

18

is 3-5 times thinner than on the edge plane (~35 nm) (Figure 4b).[149] However, such a large difference in the XPS thickness between basal and edge is not supported by recent *in situ* AFM studies.[67,68] *In situ* AFM[67,68] shows that the SEI thickness on edge plane does not change greatly after the first cycle while the SEI continues to grow on the basal plane upon cycling, indicating that the SEI formed on the edge in the first cycle is already electronically insulating and ionic conducting. Examining micro-sized graphite particles (Toyo Tanso) in composite electrodes after 3.5 cycles,[63] the XPS C1s spectra (Figure 4c) reveal the presence of similar decomposition products to those detected on lithium metal and HOPG (Figures 3, 4a,b). Interestingly, the C1s spectrum (Figure 4c) of the outermost surface of the SEI on graphite particles[63] and HOPG edge[129] are similar, with the presence of oligomers and semicarbonates, suggesting that the SEI on graphite particles (containing both edge and basal planes) is dominated by the SEI on edge planes. In addition to species such as alkoxides ROLi ($LiOCH_3$ or $LiOCH_2CH_3$), other compounds like lithium succinate,[157] lithium oxalate,[157] orthoesters,[158] orthocarbonates[158] and acetals[158] (Table S3) have also been observed on carbonaceous surfaces, highlighting the complexity of the SEI. Combined XPS and impedance analyses of the SEI on graphite further support that the organic species of the outer layer with higher impedance form at higher voltages whereas inorganic components such as Li_2CO_3 and Li_2O develop below 0.3 V_{Li}.[159]

The physical origin of SEI differences (Figure 4) on the HOPG basal and edge surfaces is not well understood. One school of thought is that as lithium ions de-solvate and intercalate in-between the graphite layers at the edge,[55,160] remaining salt anions near the edge, previously weakly bonded to the Li^+ solvated cations, may decompose and form inorganic species like LiF. On the contrary, the basal planes are exposed to fewer unsolvated salt anion molecules and more "non-coordinated" solvent molecules,[71] which lead to the formation of more organic species and

19

less inorganic compounds. On the other hand, Besenhard et al.[139] (1995, Figure 3) have proposed[161,162] that solvated complexes Li(solvent)$_x$ intercalate in between the graphene layers, which subsequently decompose to form SEI at the edge. This hypothesis is supported by recent work by Shkrob et al.,[163,164] which suggest that the SEI layer formed in EC is a polymeric and dense 3D network that passivates the surface of the electrode.[163,164] On the contrary, due to the formation of different radicals, this polymerization is impeded in PC solutions leading to a permeable network of linear polymers that does not prevent further electrolyte decomposition.[163,164] Further studies are needed to test the hypotheses and provide molecular understanding on how SEI forms.

Faster charge transfer kinetics on the edge plane[165–167] than the basal plane can also facilitate electrolyte decomposition. For example, after the first electron transfer described in Figures 2a-b, cyclic carbonates can undergo ring opening leading to the formations of radicals,[14,123] which further combine to form lithium ethylene dicarbonate (LEDC)[137,143,168] or lithium butylene dicarbonate (LBDC)[14] in the case of EC. In addition, EC decomposition can proceed by two electron solvent reduction leading to the formation of Li_2CO_3 with C_2H_4 evolution.[34,169] Moreover, after the first electron transfer (Figures 2a,b), the radical linear carbonates solvents can attack other solvent molecules to form lithium alkoxides and Li_2CO_3.[170,171] These reactions involving electron transfer may explain the larger amount of carbonates and alkoxides detected on the edge compared to basal plane.[129] In contrast, the predominance of oligomers on the basal plane could arise from the polymerization of cyclic carbonate such as EC,[172,173] requiring no electrons but rather initiated by a strong Lewis acid like PF_5.[172,173] Due to their long carbon chains, we can also infer that the access of oligomers to the edge plane is also hindered, explaining their predominance on the basal plane.

EEI layer on alloying electrodes. The degradation reactions of electrolytes on Si and Sn surfaces upon lithiation and delithiation lead mainly to the formation of similar species to those on graphite and lithium, with carbonates species such as Li_2CO_3 and RCO_2Li, $ROLi$, oligomers and LiF (Figure 3).[174–182] Moreover, species unique to the electrode materials are formed such as siloxanes,[176,178] detected in the EEI layer on Si after the first discharge/charge cycle as well as SiO_xF_y detected after prolonged cycling (>10 cycles), originating from the attack of Si-O bonds at the surface by HF from $LiPF_6$ degradation.[182,183] Recently Chan et al.[175] have proposed an EEI bilayer model on silicon nanowires similar to that of lithium and graphite, with a mostly organic EEI layer close to the electrolyte and mostly inorganic close to the Si nanowire. It is important to note that the major difference between the EEI layers on graphite and alloys electrodes is that EEI layers on alloys are not confined/stabilized on the surface during the alloying/dealloying process. Instead, they form continuously on fresh surfaces prone to electrolyte decomposition. Thus, one challenge for alloy electrodes is to engineer EEI layer on particle surfaces, using for example coatings[184] and additives,[174] that can help increase the mechanical strength of the SEI films to sustain the large volume expansion upon alloying.

Similarly to graphite, where basal and edge planes have different EEI films,[55,129,149] recent work[132,185–187] has shown a strong effect of surface termination on the EEI layer on Sn[132,185] (Figure 5) and Si[186,187] crystals at voltages above lithiation (0.8-2.5 V_{Li}), although the chemical composition of the EEI film is the same regardless of the crystal termination when lithium is alloyed with Si (below 0.6-0.8 V_{Li}).[186,187] While in practice these observations above lithiation do not fully capture the EEI layer behavior during full cycling, they provide fundamental insights in the role of surface termination and echo the study on HOPG. AFM images and soft X-ray

absorption (XAS) measurements at the F-K edge of the tetragonal β-Sn(001) (Figure 5c) reveal the formation of a thin EEI layer composed of the inorganic compound LiF from salt decomposition on the (001) surface (Figure 5c) when the electrode is cycled two times from 2.5 to 0.8 V_{Li}. On the contrary, the EEI layer on tetragonal β-Sn(100) plane formed in the same conditions is thicker and rougher (AFM, Figure 5c), and consists mostly of carbonates, as demonstrated by the predominance of Li_2CO_3 on the C-K profile in Figure 5c.[132,185] Similarly, the EEI film on the Si(100) is mainly composed of LiF and salt decomposition products while the EEI layer on the Si(111) surface consists of a mixture of carbonates.[186,187] The homogeneous thin EEI film formed on β-Sn(001) after few cycles between 0.8-2.5 V_{Li} suggests that the LiF layer is electronically insulating while the thick porous, carbonate layer on the β-Sn(100) might have continuous consumption of the electrolyte during cycling as shown by considerable reduction currents in the cyclic voltammetry scans (Figure 5d).[132,185] The difference in EEI layer composition might be explained by difference in reactivity between the two surfaces; the β-Sn(001) has a lower coordination (3 or 5 compared to 5 for the (100) surface), reflected in a surface energy 1.25 times greater for the β-Sn(001) and higher surface roughness than the β-Sn(100) (Figures 5a,b),[132,188] see SI for details on Si. It was hypothesized that the higher surface energy for the β-Sn(001) could favor a catalytic decomposition of $LiPF_6$ to LiF,[132] but no experimental evidence was provided. While the studies on HOPG, Si and Sn described here clearly reveal preferential electrolyte decomposition paths on defined surfaces, further studies are needed to elucidate the mechanisms at work.
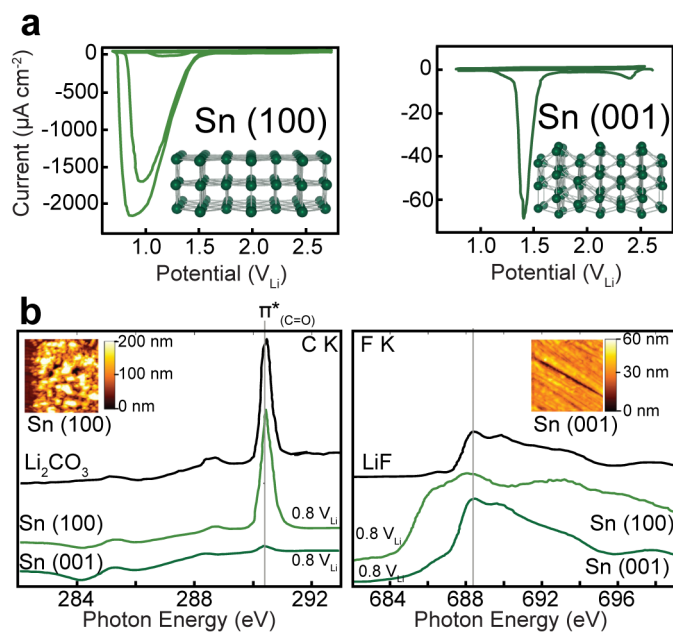
Figure 5. a) CV measurements on tetragonal β-Sn (100) and β-Sn (001) from 2.8 to 0.8 V_{Li} at 1mV s^{-1} in 1M LiPF$_6$, EC:DEC 1:2 electrolyte, showing higher cathodic current for β-Sn (100).[132] The inserts show atomic arrangement of the tetragonal β-Sn (100) and (001) surfaces, respectively. b) C-*K* (left) and F-*K* (right) edge Soft X-ray Absorption Spectroscopy (XAS) of the SEI on the β-Sn(100) and (001) surfaces after few CV between 0.8-2.5 V_{Li} (note that 0.8 V_{Li} is above the lithiation potential of Sn).[132] The β-Sn(100) consists mostly of porous carbonate while the β-Sn(001) consists mostly of LiF. The inserts are *in situ* AFM images of the β-Sn(100) and (001) surfaces at 2.5 V_{Li} after cycling twice from 2.5 V_{Li} to 0.8 V_{Li},[185] showing that the SEI on the (100) surface is rougher and thicker than the (001).[185]

Towards understanding of the EEI layer on positive electrodes. In contrast to negative electrodes, where aprotic electrolytes are thermodynamically unstable against electrochemical reduction, and the formation of SEI is critical to passivate the electrode surface

23

and enable high coulombic efficiency, there is no thermodynamic driving force for electrolyte electro-oxidation on most conventional positive electrode materials (Figure 2a). A few studies have reported surface films or EEI layers on positive electrode materials, and selected studies that show the evolution of our understanding on the EEI layers of positive electrodes are shown in Figure 6 (Figure 6 is not an exhaustive representation of previous studies on positive electrode EEI layers). Goodenough et al.[42] were one of the first to suggest the presence of EEI layers on a positive electrode, and numerous studies have tried later on to characterize it and speculated on its origin. The EEI layers on positive electrodes generally consist surprisingly of similar solvent and salt decomposition products to those found on negative electrodes,[40,58,189,190] although the EEI layer results mostly from chemical reactions (e.g. nucleophilic attack) mainly driven by the surface chemistry of the electrode material. Kanamura et al.[191] show the presence of carboxylate groups (O-C=O) on cycled $Li_{1-x}CoO_2$ using *in situ* FTIR while Aurbach et al.[64,192] report the presence of semicarbonates ($ROCO_2Li$) on the surfaces of cycled $Li_{1-x}MO_2$ and $Li_{1-x}Mn_2O_4$ electrodes (Figure 6), deriving from nucleophilic reactions of the electrode surfaces with electrolyte (see discussion below).[41,64] Recently Yabuuchi et al.[46] introduce the possible influence of O_2 release from Li-rich layered oxides ($0.5Li_{2-x}MnO_3 \bullet 0.5Li_{1-x}Co_{0.33}Ni_{0.33}Mn_{0.33}O_2$ or $Li_{1.2}$ $_xCo_{0.13}Ni_{0.13}Mn_{0.54}O_2$)) upon charging, which can be reduced to superoxide to attack carbonate solvents to form Li_2CO_3. We will discuss this mechanism in detail below. The development of *in situ* techniques on model surfaces of positive electrodes, with *in situ* neutron reflectometry on $Li_{1-x}Mn_{1.5}Ni_{0.5}O_4$[81] and *in situ* synchrotron XPS[83] and XAS[82,83,193] on $LiCoO_2$[82,193] or $Li_{1-x}Ni_{0.2}Co_{0.7}Mn_{0.1}O_2$[83] for example (Figure 6), has the potential to provide new information on EEI layers formed on the positive electrode material surfaces without the influence of carbon or

binder. A particular attention is also paid recently on the evolution of the material structure and electronic structure on the extreme surface in contact with the electrolyte.

2015
Cherkashinin et al.[83]

2014
In situ neutron reflectometry
Browning et al.[81]

2011
Yabuuchi et al.[46] $Li_{1.2-x}Ni_{0.13}Co_{0.13}Mn_{0.54}O_2$

2009
$Li_{1-x}CoO_2$
Lu et al.[78]

2000
Aurbach et al.[192]

2004
$Li_{1-x}Ni_{0.8}Co_{0.2}O_2$
Edström et al.[40]

2002
$Li_{1-x}Mn_2O_4$
Eriksson et al.[60]

1998
Evidence of ROCO$_2$Li on the surface of $Li_{1-x}MO_2$ and $Li_{1-x}Mn_2O_4$ electrodes by FTIR
Aurbach et al.[64]

1996
Detection of species with carboxylate groups on $Li_{1-x}CoO_2$ by in situ FTIR
Kanamura et al.[191]

1985
$Li_{1-x}CoO_2$
suggestion of surface layer on positive
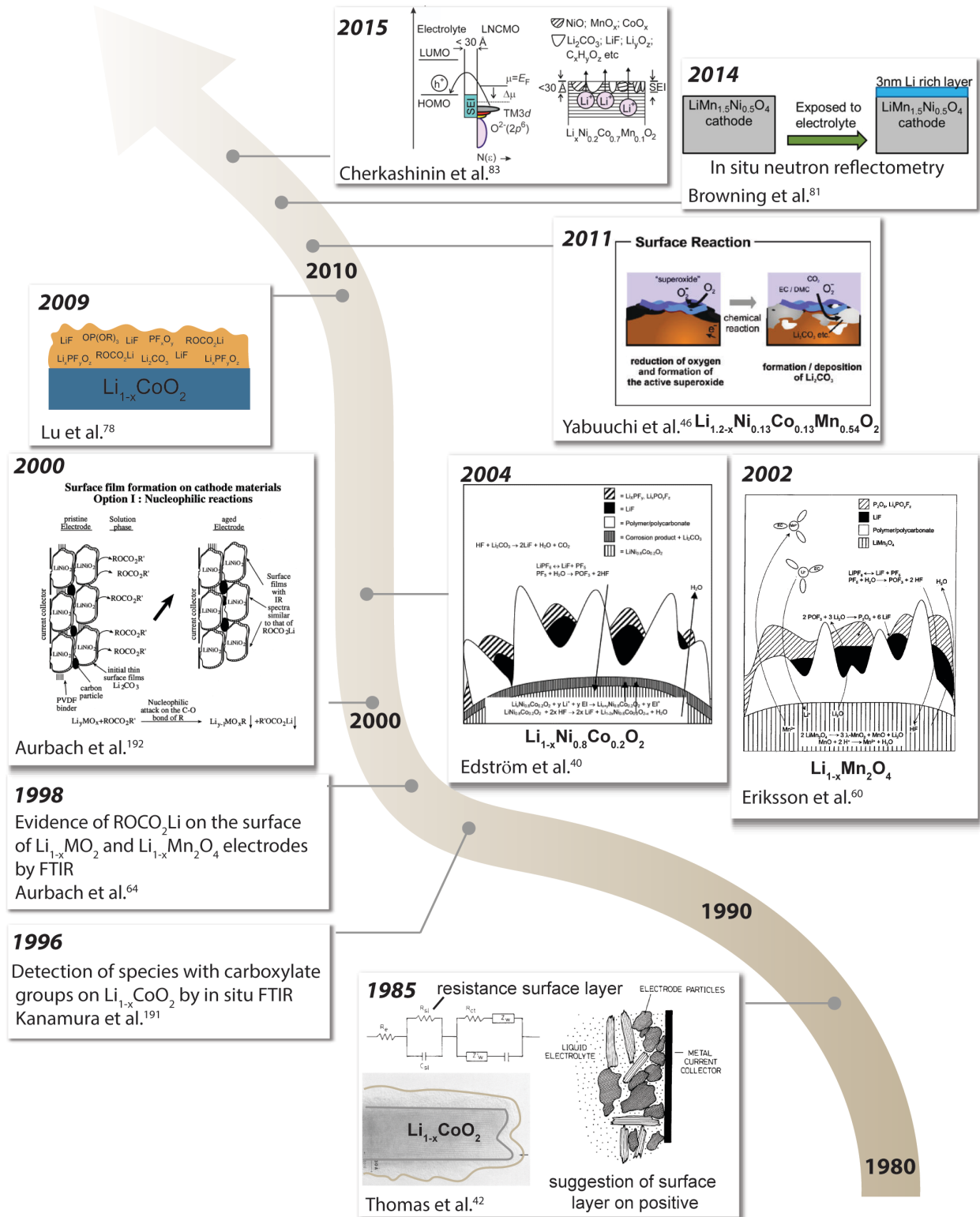Thomas et al.[42]

25

Figure 6. Investigation of the EEI layers formed on positive electrodes in the past decades. Goodenough et al.[42] first report a surface layer on charged $Li_{1-x}CoO_2$. Kanamura et al.[191] and Aurbach et al.[64,192] further report respectively carboxylates on $Li_{1-x}CoO_2$ and $ROCO_2Li$ on $Li_{1-x}MO_2$ and $Li_{1-x}Mn_2O_4$ electrodes. EEI layer models of cycled oxide electrode composites are further developed from XPS studies including Erikkson et al.[60] (2002), Edström et al.[40] (2004) and Lu et al. (2009).[78] Further study is necessary to understand the influence of oxygen release from high-capacity Li-rich oxides upon charging on the formation of Li_2CO_3 in the EEI layers (Yabuuchi et al.,[46] 2011). Recent use of *in situ* techniques on model surfaces of positive electrodes (Browning et al.,[81] Cherkashinin et al.)[83] has provided insights into the composition and thickness of EEI layers. Reproduced with permission from ref 42. Copyright 1985, The Electrochemical Society. Reprinted from refs 40,64 with permission from Elsevier. Reprinted with permission from refs 46,60,81,83.

Electronic and structural changes on the surface of positive electrodes. While most of the studies focus on the degradation of the electrolyte and on the formation of surface films on positive electrodes, the active material itself is subjected to changes such as reduction of the transition metal oxidation state[82,193] or surface reconstruction in contact to the electrolyte.[194-197] For example, upon immersion in electrolyte, cobalt ions on the surface of $LiCoO_2$ are irreversibly reduced from Co^{3+} to Co^{2+} leading locally to a distorsion of the structure.[82,193] Modification of the structure of the material are also observed in different NMC or NCA such as $LiNi_{0.4}Mn_{0.4}Co_{0.18}Ti_{0.02}O_2$[194] and $LiNi_{0.5}Co_{0.2}Mn_{0.3}O_2$[195] or $LiNi_{0.8}Co_{0.15}Al_{0.15}O_2$.[196] In $LiNi_{0.4}Mn_{0.4}Co_{0.18}Ti_{0.02}O_2$,[194] a transition from $R\overline{3}m$ to $Fm\overline{3}m$ occurs on the surface by simple contact with electrolyte or upon cycling, leading also to a reduction of the transition metals while

a surface layer of electrolyte decomposition based of LiF surrounded by organic compounds is formed on the extreme surface. Similarly, in $LiNi_{0.5}Co_{0.2}Mn_{0.3}O_2$[195] or $LiNi_{0.8}Co_{0.15}Al_{0.15}O_2$,[196] the layered structure transforms to spinel and to a NiO type structure ($Fm\overline{3}m$) on the outermost surface of the particles. The formation of the NiO on the surface is exarcerbated by cycling at high potential and supossedly increases the charge transfer resistance of the electrode as NiO is ionically resistive.[195] Changes of transition metal oxidation state and structure on the surface seem both to partially explain the degradation of the performance upon cycling.[82, 193-197]

EEI films derived from electrolyte salt decomposition. The use of $LiPF_6$ salt can lead to an increase of the impedance by 2 to 5 times on positive electrodes (Figure 7a) relative to $LiAsF_6$, which is likely due to its decomposition to LiF on the electrode surface[172] (LiF detected by XPS[41] on $Li_{1-x}NiO_2$). $LiPF_6$, the most widely used salt, can decompose in presence of water according to $LiPF_6 \rightarrow LiF + PF_5$ and $PF_5 + H_2O \rightarrow PF_3O + 2HF$, forming HF.[191] HF can in fact react with Li_2CO_3 in the EEI layers on the positive (and also on negative) electrodes, dissolving them away, and forming LiF films on the surface that are highly ionically resistive.[198,199] $LiAsF_6$ and $LiC(So_2CF_3)_3$, however, seem to not suffer from HF formation, seemingly explaining the lower impedance observed when these salts are used (Figure 7a).[41] In addition to its reactivity towards carbonates, HF can also favor dissolution of transition metals present in the positive electrode,[189,200,201] and the transition metals can migrate and be reduced on the negative electrode surface, contributing to the SEI.[202] Furthermore, phosphorous oxides (e.g. $Li_xPF_yO_z$, organophosphates ($OP(OR)_3$)) resulting from $LiPF_6$ degradation have been found on layered and spinel metal oxide composite electrodes. Their concentration increases upon cycling, similarly to LiF.[59–61,78] The detrimental influence of HF on the surface reactivity of lithium oxides can be overcome by the use of coatings such as Al_2O_3[203–205] or $AlPO_4$,[78,205] that act as a physical barrier

for HF corrosion and scavenge HF present in the electrolyte solution by promoting the formation of metal fluorides (MF_2) or oxyfluorides (M-O-F) species on the surface, which act as protective barrier against reactions of the active material with electrolyte.[78]

Nucleophilic attack of electrolytes on Li_{1-x}(Co, Ni, Mn)O_2 and $Li_{1-x}Mn_2O_4$ surfaces. Cycled layered $Li_{1-x}CoO_2$ ($Co^{3+/4+}$) and $Li_{1-x}NiO_2$ ($Ni^{3+/4+}$) display much higher impedance than spinel $Li_{1-x}Mn_2O_4$ ($Mn^{3+/4+}$) up to ten times for $Li_{1-x}NiO_2$ in F-containing electrolytes, as shown in Figure 7a.[41,205] The higher impedance of layered $Li_{1-x}MO_2$ (M = Ni and Co)[41,205] electrodes can be attributed to more carbonates (such as Li_2CO_3, polycarbonates and semicarbonates $ROCO_2Li$) and oligomers/polymers (C-O, C-C and C-H) on the surface than $Li_{1-x}Mn_2O_4$[59,60] as indicated by the C 1s XPS spectra[61,78] (Figure 7b). While the amounts of oligomers/polymers appear to increase during cycling, it is not apparent if carbonates increase during cycling[78] relative to fresh electrodes without exposure to the electrolyte, as the CF_2 signals from the PVDF binder in the composite electrode overlap with those from carbonates in the C1s spectra (Figure 7b). In contrast, negligible carbonates but some amount of oligomers/polymers (C-O, C-C and C-H) such as polyethylene oxide (PEO, polyether)[40,59] are detected for cycled $Li_{1-x}Mn_2O_4$ electrodes, as indicated by the appearance of a high-energy shoulder for the 284.5 eV peak (-C-C-) in the C1s spectra (Figure 7b).[59,60] The large increase of O-containing species present at high binding energies on the O1s spectra between fresh and cycled layered electrodes is attributed mainly to an increase of $Li_xPF_yO_z$ species from salt decomposition.[59–61,78] Indeed, in both spinel $Li_{1-x}Mn_2O_4$ and layered $Li_{1-x}CoO_2$ and $Li_{1-x}Ni_{0.8}Co_{0.2}O_2$,[59–61,78] F 1s and P 2p XPS spectra reveal the presence of $Li_xPF_yO_z$ and LiF resulting from $LiPF_6$ decomposition.

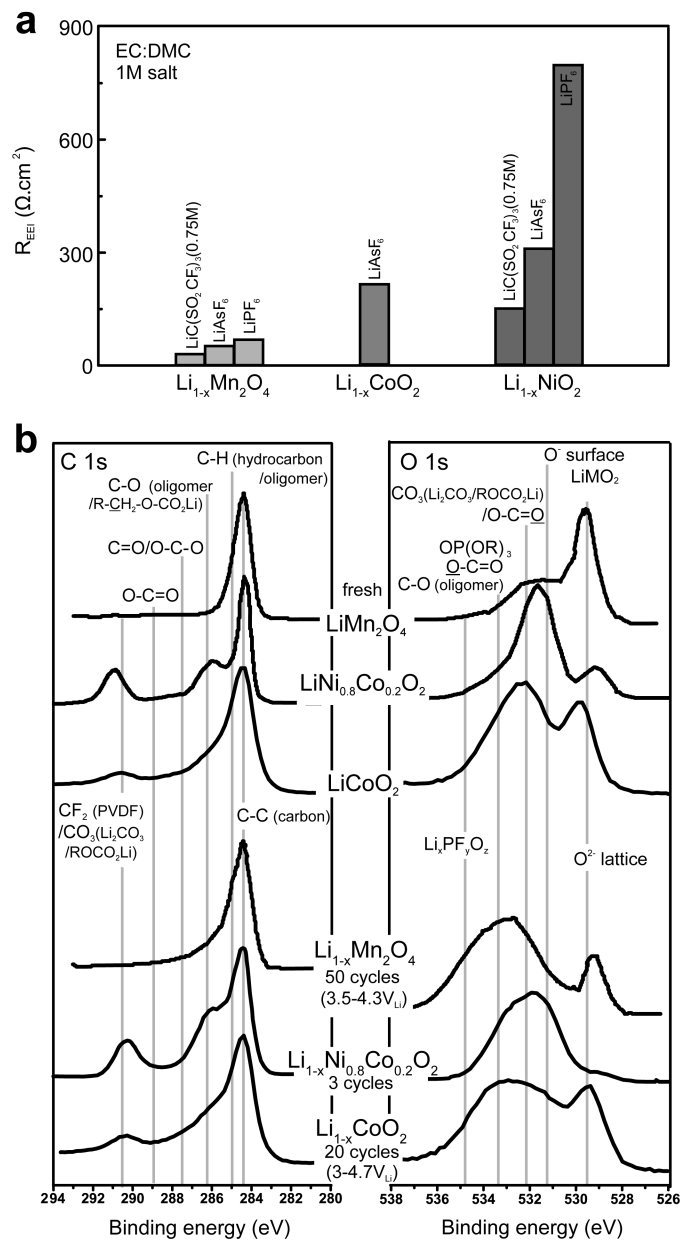**Figure 7.** a) Resistance of the EEI layer for $Li_{1-x}Mn_2O_4$,[41] $Li_{1-x}CoO_2$[205] and $Li_{1-x}NiO_2$[41] composite electrodes after few cycles (unspecified number of scans) to ~4 V_{Li} with different salts in 1:1 EC:DMC ($LiMn_2O_4$ and $LiNiO_2$) or 1:3 EC:DMC ($LiCoO_2$) (see SI for details). b) C 1s and O 1s spectra for $Li_{1-x}Mn_2O_4$,[59,60] $Li_{1-x}Ni_{0.8}Co_{0.2}O_2$[61] and $Li_{1-x}CoO_2$[78] for freshly prepared composite electrodes (no contact with electrolyte) and after 50, 3 or 20 cycles (stopped in discharge at 3.5, 3

and 2.5 V_{Li}) in 1 M $LiPF_6$ in EC:DMC 2:1, EC:DEC 1:1 and EC:DMC 1:1 respectively. Note that a non-fluorinated binder is used in the case of $LiMn_2O_4$ (ethylene propylene diene terpolymer (EPDM)), explaining the absence of CF_2 signals from the polyvinylidene fluoride (PVDF) on the C1s spectra of $Li_{1-x}Mn_2O_4$[59,60] in contrast to the CF_2 signals from the PVDF in the C1s spectra for the layered electrodes.

The greater impedance and reactivity of layered $Li_{1-x}NiO_2$ than $Li_{1-x}CoO_2$ can be attributed to higher nucleophilicity of oxygen on the $Li_{1-x}NiO_2$ surface (Figures 7 and 8),[41,64,207] which can decompose electrolyte solvent molecules through chemical (non electrochemically driven) reactions to form EEI layers with higher resistivity. Increasing the transition metal d electron filling in layered $LiMO_2$ from M=Co to Ni has been shown to increase the impedance of positive electrodes,[41,206] as shown in Figure 7a. The nucleophilicity or Lewis basicity of the oxygen on the surface corresponds to the ability of the oxygen ion to donate a pair of electrons to form a new chemical bond with a solvent molecule, which is often referred to as nucleophilic attack (Figure 8b). Generally speaking, the nucleophilicity or basicity of the oxygen on metal oxide surfaces increases with greater electronegativity (for example Ni>Co) and greater covalency of M-O bonds. We propose that the ability of the oxygen ions in layered $LiMO_2$ to donate electrons from its O p band and to attack a solvent molecule via nucleophilic interactions is thus increased from early to late metal ions, as the O p band move to higher energies (Figure 8a). The nucleophilicity of oxygen ions can thus be greater in $Li_{1-x}NiO_2$ than $Li_{1-x}CoO_2$ (Figure 8a). This hypothesis is supported by previous findings in that the nucleophilicity or Lewis basicity of oxygen in metal oxides such as MgO, SrO and CaO increases by moving the position of the O p band on the absolute energy scale (Figure 8a).[208] The nucleophilic attack leads to ring opening of cyclic carbonate (Figure 8b) and solvent decomposition, mostly triggering the formation of

semicarbonates and Li alkoxides (ROLi).[41] Caution should be taken when considering what EEI layers are formed on oxide surfaces and how carbon and binder in the composite electrodes used in these previous studies influence EEI layer composition and properties. Further experimental studies of model oxide electrodes (without carbon and binder) are needed to test previous findings and evaluate the reactivity of the active material alone towards the electrolyte. Recent applications of *in situ* techniques on model surfaces of positive electrodes have revealed new insights into the EEI layer composition and thickness. For example, Browning et al.[81] use *in situ* neutron reflectometry to reveal that EEI layers on $Li_{1-x}Mn_{1.5}Ni_{0.5}O_4$ thin films are ~3 nm in thickness and predominated by fluorides and P-O-containing species. Cherkashinin et al.[83] employ *in situ* synchrotron XPS and XAS to show EEI layers on cycled $Li_{1-x}Ni_{0.2}Co_{0.7}Mn_{0.1}O_2$[83] thin films (involving no oxygen anionic redox) that are ~3 nm in thickness and consist of lithium oxides, fluorides and carbonates.
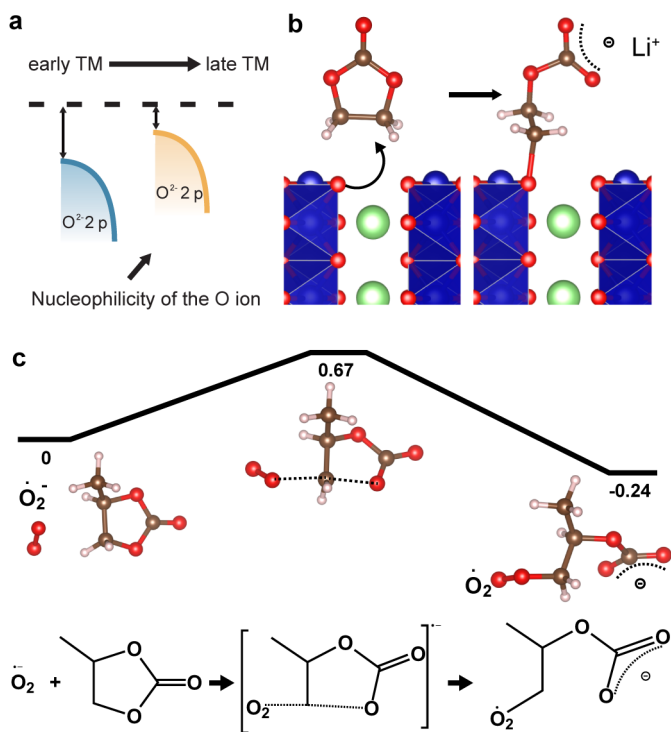

31

Figure 8. Nucleophilic attack of aprotic electrolytes on oxides. a) The difference between the Fermi level and the O p band became smaller for late transition metal oxides, which destabilizes the oxygen energy levels, and enhances the nucleophilicity of the oxygen on the surface of the electrode. b) Example of nucleophilic attack of an EC molecule by surface oxygen ions of a layered lithium transition metal oxide. (c) Reaction profiles (free energies reported in eV) for a nucleophilic attack of PC solvent by superoxide as reported in Bryantsev et al.[89]

Nucleophilic attack of electrolytes associated with oxygen anionic redox of high-capacity positive electrodes. The reactivity towards the electrolyte of layered oxides exhibiting anionic redox is not well understood. Lattice oxygen redox can produce O^- with a ligand hole in the O p band from O^{2-}, oxygen release (O^{2-} to O_2), and oxidation of O^{2-} to peroxo O_2^{2-} at the surface of layered electrodes such as $Li_{1-x}MO_2$, $Li_{2-x}MO_3$, $yLi_{2-x}MnO_3 \bullet (1-y)Li_{1-x}MO_2$) (also called Li-rich $Li_{1+y}M_{1-y}O_2$). These reactive oxygen species can oxidize carbonate electrolytes and generate EEI films. When the redox energy levels of transition metal ions pin or fall below the top of oxygen p band (Figure 9c), there is a thermodynamic driving force for oxygen redox in addition to redox of transition metals. This concept has been proposed for layered oxides such as $Li_{1-x}CoO_2$,[2,118] $Li_{1-x}NiO_2$,[2] $Ni_{1-x}CoO_2$[118] and $Na_{1-x}CoO_2$[119] up charging to voltages greater than ~4.2 V_{Li}[208] and at low concentrations of lithium or sodium, where the Co^{3+}/Co^{4+} and Ni^{3+}/Ni^{4+} couples pin at the top of O p band (Figure 9c). The oxidation of O^{2-} to O^- can proceed by forming ligand hole in the O p band, which can lead to the formation of peroxide anions O_2^{2-}[2,118,119] on the surface. These peroxide anions on the surface can react further to form molecular oxygen.[2,119–121] Although no experimental evidence had been reported for years for oxygen anion redox to form surface O^-

and O_2^{2-}, differential electrochemical mass spectrometry (DEMS) measurements clearly reveal oxygen release from selected layered $Li_{1-x}MO_2$ and $yLi_{2-x}MnO_3 \bullet (1-y)Li_{1-x}MO_2$ (Li-rich $Li_{1+y}M_{1-y}O_2$) (Figure S2).[45,47,210–212]

Reversible redox of oxide anions and peroxide anions has been demonstrated recently in the bulk lattice of $Li_{2-x}Ru_{1-y}M_yO_3$ (with M= Mn, Ti or Sn) by Tarascon's group.[48,49,117,213] For example, the first plateau of lithium de-intercalation from $Li_{2-x}Ru_{0.75}Sn_{0.25}O_3$ (Figure 9a) occurs at 3.6 V_{Li} and corresponds to the oxidation of Ru^{4+} to Ru^{5+} while the second plateau at 4.2-4.3 V_{Li} (Figure 9a) can be attributed to the oxidation of the lattice oxygen to O_2^{n-} species (Figure 9d).[49,213] In addition, only small amounts of O_2 molecules have been detected in the first charge of $Li_{2-x}Ru_{1-y}M_yO_3$ (with M= Mn or Sn) (Figures 9b), suggesting that the reaction of O_2^{2-} to form $O_{2(gas)}$ might be operative on the surface. The kinetics of evolving O_2 molecules from $Li_{2-x}Ru_{1-y}M_yO_3$ are much reduced relative to layered $Li_{1-x}CoO_2$, and replacing Mn^{4+} in $Li_{2-x}Ru_{1-y}M_yO_3$ with Sn^{4+} reduce the evolution kinetics as shown by its higher onset potential for O_2 release (Figure S3).

$yLi_{2-x}MnO_3 \bullet (1-y)Li_{1-x}MO_2$ composites or Li-rich $Li_{1+y}M_{1-y}O_2$ layered oxides can also exhibit oxygen evolution and reversible oxygen redox upon charging to high voltages ($\sim$ 4.5 V_{Li}),[214,215] as shown in Figures 9b and 9c. While the first charge plateau of Li-rich layered oxides such as Li-rich NMC[47,212] and $0.5Li_{2-x}MnO_3 \bullet 0.5Li_{1-x}Mn_{0.5}Ni_{0.5}O_2$ ($Li_{1.2}Mn_{0.6}Ni_{0.2}O_2$)[45,211] corresponds to oxidation of transition metal ions, the second plateau at $\sim$4.5 V_{Li} (Figure 9a), can be attributed to an irreversible $O_{2(g)}$ loss similar to $Li_{2-x}MnO_3$, as demonstrated by DEMS (Figures 9b, S4).[45,216,217] A significant amount of O_2 is released from the layered Li_2MnO_3[45,217] (where Mn^{4+} ions are present), coinciding with the plateau at $\sim$ 4.5 V_{Li} on the first charge of the material (Figure 9a). The higher onset potential for O_2 release at room temperature is observed for Li-rich NMC

33

$(0.1Li_{2-x}MnO_3 \bullet 0.9Li_{1-x}Ni_{0.33}Mn_{0.33}Co_{0.33}O_2$[212] and $0.5Li_{2-x}MnO_3 \bullet 0.5Li_{1-x}Mn_{0.5}Ni_{0.5}O_2$, $\sim$ 4.7-4.8 V_{Li}, Figure S3), while $0.5Li_{2-x}MnO_3 \bullet 0.5Li_{1-x}Mn_{0.5}Ni_{0.5}O_2$ ($Li_{1.2}Mn_{0.6}Ni_{0.2}O_2$) compounds present onset potentials around 4.5-4.6 V_{Li}.[211,218] Although rigorous analyses of the thermodynamics and kinetics of oxygen release across different layered oxide electrodes is challenging as different oxide preparation methods and different DEMS measurement conditions have been used, adding Mn ions in the layered oxides appears to impede oxygen release at voltages lower than 4.5 V_{Li} (Figure S2). It is interesting to note that adding Mn^{3+} ions in the parent structure of $LiNiO_2$ increases the thermal stability of the compound by increasing the onset temperature by 50 ℃ for oxygen release (Figure S3).[219] Similarly, $Li_{0.2}Ni_{0.5}Mn_{0.5}O_2$[220] releases O_2 at a $\sim$ 100 ℃ higher temperature than $Li_{0.3}NiO_2$.[219] This observation suggests that the trends in the thermodynamics and kinetics of oxygen release from charged layered oxides during heating might be comparable to those of oxygen release as a function of potential (Figure S3). This proposed correlation can be rationalized by the following argument: pushing down the Fermi level of layered oxides closer to the O p band center can destabilize oxides and promote oxygen release under highly oxidizing conditions (DEMS measurements at high charging voltages), so as make the oxide reduced easily to release oxygen under reducing conditions (thermal analysis in presence of Ar).[219] Further studies are needed to examine the universality of this proposed correlation.
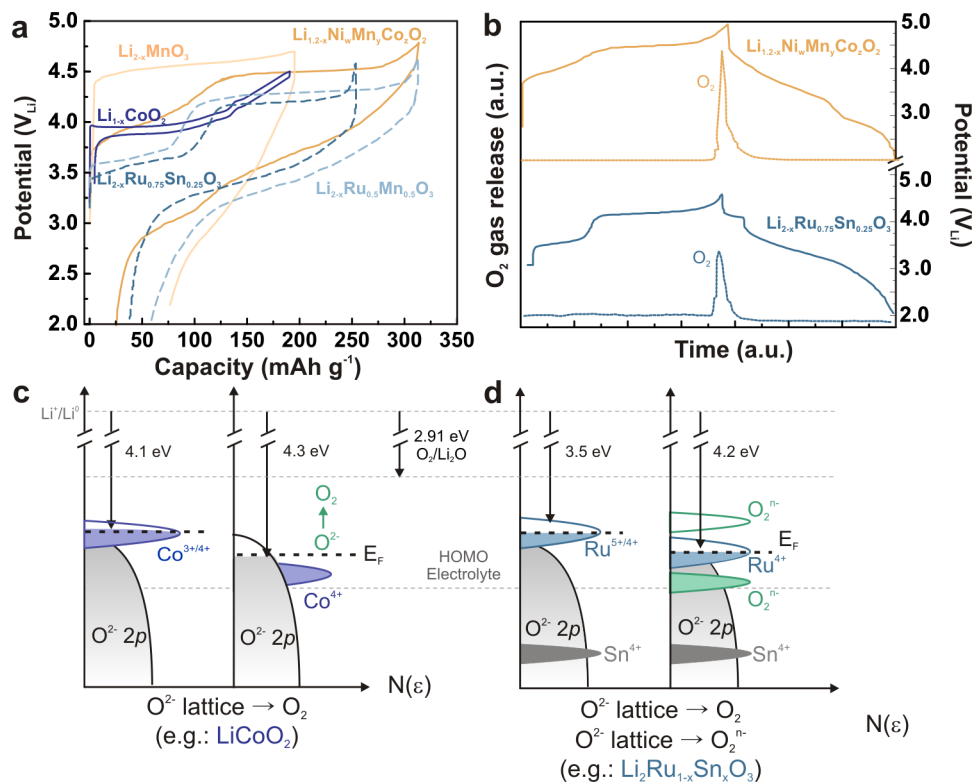
Figure 9. a) Charge/discharge curves of $Li_{1-x}CoO_2$ (C/20),[110] $0.5Li_{2-x}MnO_3 \bullet 0.5Li_{1-x}Ni_wMn_yCo_zO_2$ ($Li_{1.2-x}Ni_wMn_yCo_zO_2$) (C/10),[47] $Li_{2-x}MnO_3$ (C/28),[218] $Li_{2-x}Ru_{0.5}Mn_{0.5}O_3$ (C/20)[48] and $Li_{2-x}Ru_{0.75}Sn_{0.25}O_3$ (C/10).[49] Materials evolving oxygen release or reversible anionic redox of oxygen are represented by straight and dashed lines respectively. b) Evolution of potential and O_2 gas release (arbitrary units) measured by differential electrochemical mass spectrometry (DEMS) for $0.5Li_{2-x}MnO_3 \bullet 0.5Li_{1-x}Ni_wMn_yCo_zO_2$ ($Li_{1.2-x}Ni_wMn_yCo_zO_2$)[47] and $Li_xRu_{0.75}Sn_{0.25}O_3$.[49] Note that the relative intensities of O_2 release are arbitrary and are therefore not comparable. c) Schematic of oxygen evolution occurring during charging at high potential of $Li_{1-x}CoO_2$ due to the overlap of the Fermi level with the O p band.[2] d) Schematic of the anionic reversible oxidation occurring during charge at high potential for $Li_{2-x}Ru_{1-y}Sn_yO_3$.[49]

Oxygen release from layered $LiMO_2$, Li-rich $yLi_{2-x}MnO_3 \cdot (1-y)Li_{1-x}MO_2$ (or $Li_{1+y}M_{1-y}O_2$) and Li_2MO_3 upon charging to high voltages can trigger the nucleophilic attack of carbonate electrolytes by superoxide (O_2^-), which can form upon discharge to 3 V_{Li} and lower, which leads to EEI films formation[46] in addition to the nucleophilic attack of the electrolyte on oxide surfaces discussed above (Figures 7 and 8a,b). The implication of such nucleophilic attack by superoxide on the EEI layer formation has been first discussed by Yabuuchi et al.,[46] as shown in Figure 6, and the release of oxygen from the Li-rich materials has been recently shown to catalyze electrolyte decomposition.[221] Pioneering work by Aurbach et al.[84] and recent work on Li-oxygen batteries[85–88] have shown that superoxide (O_2^-) can attack carbonate solvents, forming inorganic species such as Li_2CO_3 or RCO_2Li and $R(OCO_2Li)_2$. Generally speaking, organic solvents can in fact be subject to two decomposition mechanisms in presence of superoxide (O_2^-) species: nucleophilic attack and proton extraction. Carbonates are not stable against superoxides as nucleophilic reactions between superoxide and carbonates (Figure 8c) are among the most thermodynamically favorable compared with other organic solvents such as amides and nitriles (Figure S4a).[89,222] Considering that the kinetics (free energy barrier, $\Delta G^{\ddagger}_{activation}$) of nucleophilic attack of carbonate molecules by superoxide scales with thermodynamic driving force ($\Delta G_{reaction}$), the reaction rates are high (Figure S4a).[89,222] In addition, the reaction of superoxide and electrolyte solvents may involve a proton abstraction from the solvent, which acts as weak acid (Brønsted) (Figure S4b). For carbonates such as PC, the proton abstraction with superoxide is less likely than nucleophilic attack since the proton abstraction is less thermodynamically favorable and is impeded by a higher activation energy (Figure S4c).[89] Combined experimental and computational findings have indicated that solvents with pKa ($\Delta G_{deprotonation}/2.303RT$) values measured in DMSO greater than 30 are expected to be stable against H^+ abstraction by

superoxide, as shown in Figure S4c.[90] Moreover, electrolytes such as ethers and glymes can be oxidized chemically by molecular O_2, which can be initiated by hydrogen (H) abstraction to form a HOO radical.[223] These reactions highlight that several requirements, ranging from the energy of HOMO/LUMO, resistance to nucleophilic attack, and appropriate values of pKa, now have to be considered to be used in conjunction with high-energy positive electrodes that potentially evolve oxygen species.[91] Besides, questions remain concerning whether the peroxide-like species at the surface of $Li_{2-x}Ru_{1-y}M_yO_3$ will react through similar mechanisms or involve different degradation reactions of the electrolyte that will contribute to the growth of EEI films. The emergence of these compounds opens new computational/experimental avenues to evaluate EEI film compositions and structures and electrolyte decomposition reaction mechanisms associated with these oxidative species at the surface of the positive electrodes for Li-ion batteries.

Future Work and New Directions. In this perspective, we review accumulated findings on the composition and properties of EEI layers on negative and positive electrodes in Li-ion batteries in the past four decades. For negative electrodes, we discuss the evolution of experimental observations and models to support the current mosaic structure for SEI on lithium and carbon, which consists of multiple inorganic and organic products from electrolyte decomposition: near the lithium surface, compact layers are formed of inorganic species like Li_2O, Li_2CO_3, and LiF, thermodynamically stable against lithium;[27,29,31,56] near the electrolyte, the layers consist mainly of oligomer species and semicarbonates.[27,29,31,56] In addition, we show how electrolyte salt, aprotic solvent and surface orientations can greatly influence the compositions and impedance of SEI. Moreover, we compare EEI layers found on alloying negative electrodes with SEI of lithium and graphite, where similar reaction products have been reported but much

greater electrode impedance or voltage polarization is needed. While a consensus exist in the community on the composition and protective nature of the SEI on negative electrodes, questions remain on the validity of previous results due to the sensitivity of the electrodes against moisture/air and on the real properties of transport of such a mosaic structure, partially composed of highly resistive materials such as LiF.[77]

The understanding of EEI layers is scarce on the positive electrode side. We discuss three different chemical reaction mechanisms at oxide electrodes that can give rise to different reaction products. First, the decomposition of electrolyte salts can greatly influence the composition and properties of EEI layers. For example, the use of $LiPF_6$ salt can lead to an increase of the impedance by 2 to 5 times on positive electrodes relative to $LiAsF_6$. Second, we highlight the critical role of the electrode surface towards electrolyte oxidation, particularly the oxygen anion and oxygen species, in forming EEI layers, mainly composed of carbonates, semicarbonates and LiF, involving chemical reactions such as nucleophilic attacks and decomposition of the salt. We discuss new opportunities in probing electrolyte decomposition and the formation of different EEI components by bridging our understanding on the reactivity of aprotic solvents against superoxide in the field of Li-O_2 batteries with that of layered $LiMO_2$, Li-rich $yLi_{2-x}MnO_3 \bullet$ (1-y)$Li_{1-x}MO_2$ (or $Li_{1+y}M_{1-y}O_2$) and Li_2MO_3. Further studies are needed to understand the effect of oxygen products such as O_2 gas, superoxide or peroxo-like species on the EEI layers, which can benefit by involving techniques such as surface-enhanced Raman, EPR[213] and DEMS[45,47,210] techniques relatively new to Li-ion battery research.

Our current understanding on SEI and EEI layers is derived largely from studies of composite electrodes that consists of additive carbon and binder, which can influence the formation of SEI/EEI layers and leads to ambiguities in the SEI/EEI layer compositions reported for electrode

materials.[197,224–226] For example, in positive electrodes, while the fraction of mass of carbon is low in composite electrodes, the surface area developed by the conductive carbon is extremely high and its reactivity towards the electrolyte could dominate the EEI on the surface of the electrode. On the other hand, the detection of similar degradation products on both negative and positive electrodes is puzzling, as different reactions (e.g. oxidation or reduction) are involved on each side. To circumvent these ambiguities, there is a need for study of model electrode surfaces such as oxide pellets and thin films, which allow for investigating the reactivity of the electrolyte with the active material surface alone. A second hurdle is the lack of information on the *dynamic* nature of the surface films formed at the EEI. The application of *in situ* or *in operando* techniques such as *in situ* XPS, XAS, surface-enhanced Raman and surface structural characterization of well-defined surfaces can capture dynamic changes of EEI layers unequivocally in its working environment. For instance, the recent development of high-pressure x-ray photoelectron spectroscopy (HPXPS) for studying the EEI layers on Si electrode[227] gives a glimpse of the exciting opportunities and unprecedented results that in situ techniques can offer. Such studies can provide insights into long standing open questions on SEI/EEI layers including: how does SEI/EEI form? What parameters can control SEI/EEI compositions? What are their properties, thickness, and uniformity at the interface? How does the process of lithium desolvation influence SEI/EEI layer formation on the electrode surface? Such understanding is required to promote Li conduction and reduce impedance through the SEI/EEI, minimize electrolyte degradation during cycling, and develop stable or predictable SEI/EEI in the lifetime of Li-ion batteries.

Guided by these questions, researchers will be able to elucidate reaction mechanisms at the EEI and develop design principles to predict and control the interfaces of Li-ion batteries.

Supporting Information. Additional information about thermodynamics of lithium insertion/deinsertion, electrolyte stability and EEI layers of positive and negative electrodes. Details of data extraction for the summary figures. This material is available free of charge via the Internet at http://pubs.acs.org.

Corresponding Author

* To whom correspondence should be addressed: shaohorn@mit.edu

Magali Gauthier is a postdoctoral associate at MIT in the Electrochemical Energy Lab. Her research focuses on interfaces in Li-ion batteries. She received her BS and MS degrees from University of Nantes and her PhD in material sciences from both University of Nantes and INRS University (Canada), researching silicon electrodes for Li-ion batteries.

Thomas J. Carney is a PhD candidate in the Department of Materials Science and Engineering at MIT. He received his BS from Stanford University where his research focused on transparent conducting electrodes and nanostructured battery materials. At MIT, his research focuses on redox flow batteries, intercalation materials, and interfacial chemistry.

Alexis Grimaud was postdoctoral associate at MIT (2012-2014) and is now associate researcher at Collège de France in Paris in Prof. Tarascon's group, focusing on the design of materials for water splitting, metal-air and Li-ion batteries. He received his engineering diploma from the Graduate School of Chemistry and Physics of Bordeaux and his PhD from the University of Bordeaux.

Livia Giordano is an assistant professor at the Material Science Department of University of Milano-Bicocca in Italy, and is currently a visiting professor at MIT. She obtained her PhD in Material Science from the University of Milano. Her research focuses on first-principles calculations of surface reactivity of oxides and metal-oxide and oxide-liquid interfaces.

Nir Pour is a postdoctoral associate at MIT in the Electrochemical Energy Lab. His research centers on vanadium redox flow batteries. He hold a BSc degree in Biophysics and an MSc and PhD. in chemistry researching magnesium batteries under the supervision of Prof. Doron Aurbach, from Bar-Ilan University in Israel.

Hao-Hsun Chang received his BS, MS, and PhD degrees in chemical engineering from National Taiwan University. His current research as a postdoctoral fellow/associate in Prof. Shao-Horn's group center on solid-state electrolytes for lithium-ion and metal-air batteries. Previously, he was a senior engineer at China Petrochemical Development Corporation and a principal engineer at Taiwan Semiconductor Manufacturing Company.

David P. Fenning is an Assistant Professor in the NanoEngineering Department at UC San Diego. His research focuses on designing materials and architectures for solar energy conversion and storage. Previously, after a PhD in solar cell defect engineering at MIT, he worked on photoelectrochemistry as an MIT/Battelle postdoc in the MIT Electrochemistry Energy Lab.

Simon Lux obtained a MSc. degree in Technical Chemistry from the Technical University of Graz and completed his PhD in Physical Chemistry at the University of Muenster. After two years at the Lawrence Berkeley National Laboratory, Simon joined BMW of North America as Advanced Battery Engineer where he is responsible for the lithium-ion battery technology projects.

Odysseas Paschos obtained his PhD from College of Nanoscale Science and Engineering at SUNY Albany and worked then at the Technische Universität München as a Post-Doctoral Associate in the Physics Department. Since 2012 he is in charge of the Material projects investigating technologies for future automotive cells at BMW in the Research Battery Technology group.

Christoph Bauer joined the Research Battery Technology group at BMW in 2012 after completing his Diploma in Physics at the Technical University of Munich. He gathered multiple years of experience in applied research including work in Singapore and San Francisco. His current research interests are in battery lifetime and performance for high energy and power applications.

Filippo Maglia received his PhD from the University of Pavia (1998) and was then assistant professor in the Chemistry Department (2005-2012). He has been a visiting scientist at the University of California Davis and was DAAD fellow at the Technische Universität München. He is currently working on lifetime aspects of battery materials at BMW AG in the "Research Battery Technology" department.

Saskia Lupart received her MSc. degree in Chemistry and PhD. in solid-state chemistry from the Ludwig-Maximilians-Universität München, Germany. Since 2012 she is working at BMW AG in the group of Dr. Lamp in the Research Battery Technology section where she is in charge of solid-state electrolytes for lithium batteries.

Peter Lamp received his MSc from the Technical University of Munich and his PhD from the Max Planck Institute for Physics, Munich. He was group leader at the Department of Energy Conversion and Storage of the Bayerischen Zentrum für Angewandte Energieforschung (ZAE) and a project leader for fuel cell systems at Webasto Thermo Systems International GmbH. He joined BMW AG in 2001 and is now the leader of the "Battery Technology" department at BMW.

Yang Shao-Horn is W.M. Keck Professor of Energy, Professor of Mechanical Engineering and Materials Science and Engineering at MIT. Her interests include surface science, catalysis/electrocatalysis, and design of materials for electrochemical energy storage, solid-state ionics and photoelectrochemical conversion. Professor Shao-Horn has published around 200 research articles and mentored/trained over 50 MS and PhD students and postdoctoral associates at MIT. http://web.mit.edu/eel/

ACKNOWLEDGMENT

REFERENCES

(1) Armand, M.; Tarascon, J.-M. Building Better Batteries. *Nature* **2008**, *451*, 652–657.
(2) Goodenough, J. B.; Kim, Y. Challenges for Rechargeable Li Batteries†. *Chem. Mater.* **2010**, *22*, 587–603.
(3) Bruce, P. G.; Scrosati, B.; Tarascon, J.-M. Nanomaterials for Rechargeable Lithium Batteries. *Angew. Chem. Int. Ed.* **2008**, *47*, 2930–2946.
(4) Yazami, R.; Touzain, P. A Reversible Graphite-Lithium Negative Electrode for Electrochemical Generators. *J. Power Sources* **1983**, *9*, 365–371.
(5) Mizushima, K.; Jones, P. C.; Wiseman, P. J.; Goodenough, J. B. Li_xCoO_2 (0<x<1): A New Cathode Material for Batteries of High Energy Density. *Mater. Res. Bull.* **1980**, *15*, 783–789.
(6) Hightower, A.; Ahn, C. C.; Fultz, B.; Rez, P. Electron Energy-Loss Spectrometry on Lithiated Graphite. *Appl. Phys. Lett.* **2000**, *77*, 238–240.
(7) Thomas, M. G. S. R.; David, W. I. F.; Goodenough, J. B.; Groves, P. Synthesis and Structural Characterization of the Normal Spinel $Li[Ni_2]O_4$. *Mater. Res. Bull.* **1985**, *20*, 1137–1146.
(8) Rossen, E.; Jones, C. D. W.; Dahn, J. R. Structure and Electrochemistry of $Li_xMn_yNi_{1-y}O_2$. *Solid State Ion.* **1992**, *57*, 311–318.
(9) Ohzuku, T.; Kitagawa, M.; Hirai, T. Electrochemistry of Manganese Dioxide in Lithium Nonaqueous Cell III. X-Ray Diffractional Study on the Reduction of Spinel-Related Manganese Dioxide. *J. Electrochem. Soc.* **1990**, *137*, 769–775.

(10) Padhi, A. K.; Nanjundaswamy, K. S.; Goodenough, J. B. Phospho-olivine as Positive-Electrode Materials for Rechargeable Lithium Batteries. *J. Electrochem. Soc.* **1997**, *144*, 1188–1194.

(11) Zhang, X.; Kostecki, R.; Richardson, T. J.; Pugh, J. K.; Ross, P. N. Electrochemical and Infrared Studies of the Reduction of Organic Carbonates. *J. Electrochem. Soc.* **2001**, *148*, A1341–A1345.

(12) Ue, M.; Ida, K.; Mori, S. Electrochemical Properties of Organic Liquid Electrolytes Based on Quaternary Onium Salts for Electrical Double-Layer Capacitors. *J. Electrochem. Soc.* **1994**, *141*, 2989–2996.

(13) Ue, M.; Takeda, M.; Takehara, M.; Mori, S. Electrochemical Properties of Quaternary Ammonium Salts for Electrochemical Capacitors. *J. Electrochem. Soc.* **1997**, *144*, 2684–2688.

(14) Wang, Y.; Nakamura, S.; Ue, M.; Balbuena, P. B. Theoretical Studies To Understand Surface Chemistry on Carbon Anodes for Lithium-Ion Batteries: Reduction Mechanisms of Ethylene Carbonate. *J. Am. Chem. Soc.* **2001**, *123*, 11708–11718.

(15) Leung, K. Two-Electron Reduction of Ethylene Carbonate: A Quantum Chemistry Re-Examination of Mechanisms. *Chem. Phys. Lett.* **2013**, *568-569*, 1–8.

(16) Xing, L.; Borodin, O.; Smith, G. D.; Li, W. Density Functional Theory Study of the Role of Anions on the Oxidative Decomposition Reaction of Propylene Carbonate. *J. Phys. Chem. A* **2011**, *115*, 13896–13905.

(17) Borodin, O.; Behl, W.; Jow, T. R. Oxidative Stability and Initial Decomposition Reactions of Carbonate, Sulfone, and Alkyl Phosphate-Based Electrolytes. *J. Phys. Chem. C* **2013**, *117*, 8661–8682.

(18) Zhang, X.; Pugh, J. K.; Ross, P. N. Computation of Thermodynamic Oxidation Potentials of Organic Solvents Using Density Functional Theory. *J. Electrochem. Soc.* **2001**, *148*, E183–E188.

(19) Egashira, M.; Takahashi, H.; Okada, S.; Yamaki, J. Measurement of the Electrochemical Oxidation of Organic Electrolytes Used in Lithium Batteries by Microelectrode. *J. Power Sources* **2001**, *92*, 267–271.

(20) Xu, K.; Ding, S. P.; Jow, T. R. Toward Reliable Values of Electrochemical Stability Limits for Electrolytes. *J. Electrochem. Soc.* **1999**, *146*, 4172–4178.

(21) Hayashi, K.; Nemoto, Y.; Tobishima, S.; Yamaki, J. Mixed Solvent Electrolyte for High Voltage Lithium Metal Secondary Cells. *Electrochim. Acta* **1999**, *44*, 2337–2344.

(22) Leung, K. Electronic Structure Modeling of Electrochemical Reactions at Electrode/Electrolyte Interfaces in Lithium Ion Batteries. *J. Phys. Chem. C* **2013**, *117*, 1539–1547.

(23) Smith, A. J.; Burns, J. C.; Trussler, S.; Dahn, J. R. Precision Measurements of the Coulombic Efficiency of Lithium-Ion Batteries and of Electrode Materials for Lithium-Ion Batteries. *J. Electrochem. Soc.* **2010**, *157*, A196–A202.

(24) Shim, J.; Kostecki, R.; Richardson, T.; Song, X.; Striebel, K. A. Electrochemical Analysis for Cycle Performance and Capacity Fading of a Lithium-Ion Battery Cycled at Elevated Temperature. *J. Power Sources* **2002**, *112*, 222–230.

(25) Menkin, S.; Golodnitsky, D.; Peled, E. Artificial Solid-Electrolyte Interphase (SEI) for Improved Cycleability and Safety of Lithium–ion Cells for EV Applications. *Electrochem. Commun.* **2009**, *11*, 1789–1791.

(26) Peled, E. The Electrochemical Behavior of Alkali and Alkaline Earth Metals in Nonaqueous Battery Systems—The Solid Electrolyte Interphase Model. *J. Electrochem. Soc.* **1979**, *126*, 2047–2051.

(27) Peled, E.; Golodnitsky, D.; Ardel, G. Advanced Model for Solid Electrolyte Interphase Electrodes in Liquid and Polymer Electrolytes. *J. Electrochem. Soc.* **1997**, *144*, L208–L210.

(28) Aurbach, D.; Markovsky, B.; Levi, M. D.; Levi, E.; Schechter, A.; Moshkovich, M.; Cohen, Y. New Insights into the Interactions between Electrode Materials and Electrolyte Solutions for Advanced Nonaqueous Batteries. *J. Power Sources* **1999**, *81–82*, 95–111.

(29) Aurbach, D.; Markovsky, B.; Shechter, A.; Ein-Eli, Y.; Cohen, H. A Comparative Study of Synthetic Graphite and Li Electrodes in Electrolyte Solutions Based on Ethylene Carbonate-Dimethyl Carbonate Mixtures. *J. Electrochem. Soc.* **1996**, *143*, 3809–3820.

(30) Fong, R.; Sacken, U. von; Dahn, J. R. Studies of Lithium Intercalation into Carbons Using Nonaqueous Electrochemical Cells. *J. Electrochem. Soc.* **1990**, *137*, 2009–2013.

(31) Peled, E.; Golodnttsky, D.; Ardel, G.; Menachem, C.; Bar Tow, D.; Eshkenazy, V. The Role of Sei in Lithium and Lithium Ion Batteries. In *Symposium W – Materials for Electrochemical Energy Storage and Conversion*; MRS Online Proceedings Library; 1995; Vol. 393.

(32) Aurbach, D.; Zaban, A. Impedance Spectroscopy of Lithium Electrodes: Part 1. General Behavior in Propylene Carbonate Solutions and the Correlation to Surface Chemistry and Cycling Efficiency. *J. Electroanal. Chem.* **1993**, *348*, 155–179.

(33) Vetter, J.; Novák, P.; Wagner, M. R.; Veit, C.; Möller, K.-C.; Besenhard, J. O.; Winter, M.; Wohlfahrt-Mehrens, M.; Vogler, C.; Hammouche, A. Ageing Mechanisms in Lithium-Ion Batteries. *J. Power Sources* **2005**, *147*, 269–281.

(34) Xu, K. Nonaqueous Liquid Electrolytes for Lithium-Based Rechargeable Batteries. *Chem. Rev.* **2004**, *104*, 4303–4418.

(35) Schranzhofer, H.; Bugajski, J.; Santner, H. J.; Korepp, C.; Möller, K.-C.; Besenhard, J. O.; Winter, M.; Sitte, W. Electrochemical Impedance Spectroscopy Study of the SEI Formation on Graphite and Metal Electrodes. *J. Power Sources* **2006**, *153*, 391–395.

(36) Yamada, Y.; Iriyama, Y.; Abe, T.; Ogumi, Z. Kinetics of Lithium Ion Transfer at the Interface between Graphite and Liquid Electrolytes: Effects of Solvent and Surface Film. *Langmuir* **2009**, *25*, 12766–12770.

(37) Aurbach, D.; Zinigrad, E.; Teller, H.; Dan, P. Factors Which Limit the Cycle Life of Rechargeable Lithium (Metal) Batteries. *J. Electrochem. Soc.* **2000**, *147*, 1274–1279.

(38) Crowther, O.; West, A. C. Effect of Electrolyte Composition on Lithium Dendrite Growth. *J. Electrochem. Soc.* **2008**, *155*, A806.

(39) Bhattacharyya, R.; Key, B.; Chen, H.; Best, A. S.; Hollenkamp, A. F.; Grey, C. P. In Situ NMR Observation of the Formation of Metallic Lithium Microstructures in Lithium Batteries. *Nat Mater* **2010**, *9*, 504–510.

(40) Edström, K.; Gustafsson, T.; Thomas, J. O. The Cathode-Electrolyte Interface in the Li-Ion Battery. *Electrochim. Acta* **2004**, *50*, 397–403.

(41) Aurbach, D.; Gamolsky, K.; Markovsky, B.; Salitra, G.; Gofer, Y.; Heider, U.; Oesten, R.; Schmidt, M. The Study of Surface Phenomena Related to Electrochemical Lithium Intercalation into Li_xMO_y Host Materials (M = Ni, Mn). *J. Electrochem. Soc.* **2000**, *147*, 1322–1331.

(42) Thomas, M. G. S. R.; Bruce, P. G.; Goodenough, J. B. AC Impedance Analysis of Polycrystalline Insertion Electrodes: Application to $Li_{1-x}CoO_2$. *J. Electrochem. Soc.* **1985**, *132*, 1521–1528.

(43) Guyomard, D.; Tarascon, J. M. Rechargeable $Li_{1+x}Mn_2O_4$/Carbon Cells with a New Electrolyte Composition Potentiostatic Studies and Application to Practical Cells. *J. Electrochem. Soc.* **1993**, *140*, 3071–3081.

(44) Lu, Z.; Dahn, J. R. Understanding the Anomalous Capacity of $Li/Li[Ni_xLi_{(1/3–2x/3)}Mn_{(2/3–x/3)}]O_2$ Cells Using In Situ X-Ray Diffraction and Electrochemical Studies. *J. Electrochem. Soc.* **2002**, *149*, A815–A822.

(45) Armstrong, A. R.; Holzapfel, M.; Novak, P.; Johnson, C. S.; Kang, S.-H.; Thackeray, M. M.; Bruce, P. G. Demonstrating Oxygen Loss and Associated Structural Reorganization in the Lithium Battery Cathode $Li[Ni_{0.2}Li_{0.2}Mn_{0.6}]O_2$. *J. Am. Chem. Soc.* **2006**, *128*, 8694–8698.

(46) Yabuuchi, N.; Yoshii, K.; Myung, S.-T.; Nakai, I.; Komaba, S. Detailed Studies of a High-Capacity Electrode Material for Rechargeable Batteries, $Li_2MnO_3–LiCo_{1/3}Ni_{1/3}Mn_{1/3}O_2$. *J. Am. Chem. Soc.* **2011**, *133*, 4404–4419.

(47) Castel, E.; Berg, E. J.; Kazzi, M. El; Novák, P.; Villevieille, C. Differential Electrochemical Mass Spectrometry Study of the Interface of xLi_2MnO_3·$(1–x)LiMO_2$ (M = Ni, Co, and Mn) Material as a Positive Electrode in Li-Ion Batteries. *Chem. Mater.* **2014**, *26*, 5051–5057.

(48) Sathiya, M.; Ramesha, K.; Rousse, G.; Foix, D.; Gonbeau, D.; Prakash, A. S.; Doublet, M. L.; Hemalatha, K.; Tarascon, J.-M. High Performance $Li_2Ru_{1–y}Mn_yO_3$ (0.2 ≤ y ≤ 0.8) Cathode Materials for Rechargeable Lithium-Ion Batteries: Their Understanding. *Chem. Mater.* **2013**, *25*, 1121–1131.

(49) Sathiya, M.; Rousse, G.; Ramesha, K.; Laisa, C. P.; Vezin, H.; Sougrati, M. T.; Doublet, M.-L.; Foix, D.; Gonbeau, D.; Walker, W.; et al. Reversible Anionic Redox Chemistry in High-Capacity Layered-Oxide Electrodes. *Nat. Mater.* **2013**, *12*, 827–835.

(50) Biensan, P.; Simon, B.; Pérès, J. P.; de Guibert, A.; Broussely, M.; Bodet, J. M.; Perton, F. On Safety of Lithium-Ion Cells. *J. Power Sources* **1999**, *81–82*, 906–912.

(51) Wang, Y.; Jiang, J.; Dahn, J. R. The Reactivity of Delithiated $Li(Ni_{1/3}Co_{1/3}Mn_{1/3})O_2$, $Li(Ni_{0.8}Co_{0.15}Al_{0.05})O_2$ or $LiCoO_2$ with Non-Aqueous Electrolyte. *Electrochem. Commun.* **2007**, *9*, 2534–2540.

(52) Yamaki, J.; Baba, Y.; Katayama, N.; Takatsuji, H.; Egashira, M.; Okada, S. Thermal Stability of Electrolytes with Li_xCoO_2 Cathode or Lithiated Carbon Anode. *J. Power Sources* **2003**, *119–121*, 789–793.

(53) Jiang, J.; Dahn, J. R. Effects of Particle Size and Electrolyte Salt on the Thermal Stability of $Li_{0.5}CoO_2$. *Electrochim. Acta* **2004**, *49*, 2661–2666.

(54) Nazri, G.; Muller, R. H. Composition of Surface Layers on Li Electrodes in PC, $LiClO_4$ of Very Low Water Content. *J. Electrochem. Soc.* **1985**, *132*, 2050–2054.

(55) Peled, E.; Bar Tow, D.; Merson, A.; Gladkich, A.; Burstein, L.; Golodnitsky, D. Composition, Depth Profiles and Lateral Distribution of Materials in the SEI Built on HOPG-TOF SIMS and XPS Studies. *J. Power Sources* **2001**, *97–98*, 52–57.

(56) Kanamura, K.; Tamura, H.; Takehara, Z. XPS Analysis of a Lithium Surface Immersed in Propylene Carbonate Solution Containing Various Salts. *J. Electroanal. Chem.* **1992**, *333*, 127–142.

(57) Kanamura, K.; Tamura, H.; Shiraishi, S.; Takehara, Z. XPS Analysis of Lithium Surfaces Following Immersion in Various Solvents Containing LiBF$_4$. *J. Electrochem. Soc.* **1995**, *142*, 340–347.

(58) Dedryvère, R.; Martinez, H.; Leroy, S.; Lemordant, D.; Bonhomme, F.; Biensan, P.; Gonbeau, D. Surface Film Formation on Electrodes in a LiCoO$_2$/graphite Cell: A Step by Step XPS Study. *J. Power Sources* **2007**, *174*, 462–468.

(59) Eriksson, T.; Andersson, A. M.; Bishop, A. G.; Gejke, C.; Gustafsson, T.; Thomas, J. O. Surface Analysis of LiMn$_2$O$_4$ Electrodes in Carbonate-Based Electrolytes. *J. Electrochem. Soc.* **2002**, *149*, A69–A78.

(60) Eriksson, T.; Andersson, A. M.; Gejke, C.; Gustafsson, T.; Thomas, J. O. Influence of Temperature on the Interface Chemistry of Li$_x$Mn$_2$O$_4$ Electrodes. *Langmuir* **2002**, *18*, 3609–3619.

(61) Andersson, A. M.; Abraham, D. P.; Haasch, R.; MacLaren, S.; Liu, J.; Amine, K. Surface Characterization of Electrodes from High Power Lithium-Ion Batteries. *J. Electrochem. Soc.* **2002**, *149*, A1358–A1369.

(62) Edström, K.; Herstedt, M.; Abraham, D. P. A New Look at the Solid Electrolyte Interphase on Graphite Anodes in Li-Ion Batteries. *J. Power Sources* **2006**, *153*, 380–384.

(63) Malmgren, S.; Ciosek, K.; Hahlin, M.; Gustafsson, T.; Gorgoi, M.; Rensmo, H.; Edström, K. Comparing Anode and Cathode Electrode/electrolyte Interface Composition and Morphology Using Soft and Hard X-Ray Photoelectron Spectroscopy. *Electrochim. Acta* **2013**, *97*, 23–32.

(64) Aurbach, D. Review of Selected Electrode–solution Interactions Which Determine the Performance of Li and Li Ion Batteries. *J. Power Sources* **2000**, *89*, 206–218.

(65) Shi, F.; Ross, P. N.; Zhao, H.; Liu, G.; Somorjai, G. A.; Komvopoulos, K. A Catalytic Path for Electrolyte Reduction in Lithium-Ion Cells Revealed by in Situ Attenuated Total Reflection-Fourier Transform Infrared Spectroscopy. *J. Am. Chem. Soc.* **2015**, *137*, 3181–3184.

(66) Nazri, G.; Muller, R. H. In Situ X-Ray Diffraction of Surface Layers on Lithium in Nonaqueous Electrolyte. *J. Electrochem. Soc.* **1985**, *132*, 1385–1387.

(67) Jeong, S.-K.; Inaba, M.; Abe, T.; Ogumi, Z. Surface Film Formation on Graphite Negative Electrode in Lithium-Ion Batteries: AFM Study in an Ethylene Carbonate-Based Solution. *J. Electrochem. Soc.* **2001**, *148*, A989–A993.

(68) Domi, Y.; Ochida, M.; Tsubouchi, S.; Nakagawa, H.; Yamanaka, T.; Doi, T.; Abe, T.; Ogumi, Z. In Situ AFM Study of Surface Film Formation on the Edge Plane of HOPG for Lithium-Ion Batteries. *J. Phys. Chem. C* **2011**, *115*, 25484–25489.

(69) Cresce, A. v.; Russell, S. M.; Baker, D. R.; Gaskell, K. J.; Xu, K. In Situ and Quantitative Characterization of Solid Electrolyte Interphases. *Nano Lett.* **2014**, *14*, 1405-1412.

(70) Inaba, M.; Kawatate, Y.; Funabiki, A.; Jeong, S.-K.; Abe, T.; Ogumi, Z. STM Study on Graphite/electrolyte Interface in Lithium-Ion Batteries: Solid Electrolyte Interface Formation in Trifluoropropylene Carbonate Solution. *Electrochim. Acta* **1999**, *45*, 99–105.

(71) Inaba, M.; Siroma, Z.; Kawatate, Y.; Funabiki, A.; Ogumi, Z. Electrochemical Scanning Tunneling Microscopy Analysis of the Surface Reactions on Graphite Basal Plane in Ethylene Carbonate-Based Solvents and Propylene Carbonate. *J. Power Sources* **1997**, *68*, 221–226.

(72) Inaba, M.; Siroma, Z.; Funabiki, A.; Ogumi, Z.; Abe, T.; Mizutani, Y.; Asano, M. Electrochemical Scanning Tunneling Microscopy Observation of Highly Oriented Pyrolytic Graphite Surface Reactions in an Ethylene Carbonate-Based Electrolyte Solution. *Langmuir* **1996**, *12*, 1535–1540.

(73) Aurbach, D.; Weissman, I.; Zaban, A.; Chusid, O. Correlation between Surface Chemistry, Morphology, Cycling Efficiency and Interfacial Properties of Li Electrodes in Solutions Containing Different Li Salts. *Electrochim. Acta* **1994**, *39*, 51–71.

(74) Peled, E.; Golodnitsky, D.; Menachem, C.; Bar-Tow, D. An Advanced Tool for the Selection of Electrolyte Components for Rechargeable Lithium Batteries. *J. Electrochem. Soc.* **1998**, *145*, 3482–3486.

(75) Dupré, N.; Martin, J.-F.; Guyomard, D.; Yamada, A.; Kanno, R. Characterization of Interphases Appearing on $LiNi_{0.5}Mn_{0.5}O_2$ Using ^7Li MAS NMR. *J. Power Sources* **2009**, *189*, 557–560.

(76) Eshkenazi, V.; Peled, E.; Burstein, L.; Golodnitsky, D. XPS Analysis of the SEI Formed on Carbonaceous Materials. *Solid State Ion.* **2004**, *170*, 83–91.

(77) Winter, M. The Solid Electrolyte Interphase – The Most Important and the Least Understood Solid Electrolyte in Rechargeable Li Batteries. *Z. Phys. Chem.* **2009**, *223*, 1395–1406.

(78) Lu, Y.-C.; Mansour, A. N.; Yabuuchi, N.; Shao-Horn, Y. Probing the Origin of Enhanced Stability of "$AlPO_4$" Nanoparticle Coated $LiCoO_2$ during Cycling to High Voltages: Combined XRD and XPS Studies. *Chem. Mater.* **2009**, *21*, 4408–4424.

(79) Nie, M.; Chalasani, D.; Abraham, D. P.; Chen, Y.; Bose, A.; Lucht, B. L. Lithium Ion Battery Graphite Solid Electrolyte Interphase Revealed by Microscopy and Spectroscopy. *J. Phys. Chem. C* **2013**, *117*, 1257–1267.

(80) Carroll, K. J.; Qian, D.; Fell, C.; Calvin, S.; Veith, G. M.; Chi, M.; Baggetto, L.; Meng, Y. S. Probing the Electrode/electrolyte Interface in the Lithium Excess Layered Oxide $Li_{1.2}Ni_{0.2}Mn_{0.6}O_2$. *Phys. Chem. Chem. Phys.* **2013**, *15*, 11128–11138.

(81) Browning, J. F.; Baggetto, L.; Jungjohann, K. L.; Wang, Y.; Tenhaeff, W. E.; Keum, J. K.; Wood, D. L.; Veith, G. M. In Situ Determination of the Liquid/Solid Interface Thickness and Composition for the Li Ion Cathode $LiMn_{1.5}Ni_{0.5}O_4$. *ACS Appl. Mater. Interfaces* **2014**, *6*, 18569–18576.

(82) Yamamoto, K.; Minato, T.; Mori, S.; Takamatsu, D.; Orikasa, Y.; Tanida, H.; Nakanishi, K.; Murayama, H.; Masese, T.; Mori, T.; et al. Improved Cyclic Performance of Lithium-Ion Batteries: An Investigation of Cathode/Electrolyte Interface via In Situ Total-Reflection Fluorescence X-Ray Absorption Spectroscopy. *J. Phys. Chem. C* **2014**, *118*, 9538–9543.

(83) Cherkashinin, G.; Motzko, M.; Schulz, N.; Späth, T.; Jaegermann, W. Electron Spectroscopy Study of Li[Ni,Co,Mn]O_2/Electrolyte Interface: Electronic Structure, Interface Composition, and Device Implications. *Chem. Mater.* **2015**, *27* (8), 2875–2887.

(84) Aurbach, D.; Daroux, M.; Faguy, P.; Yeager, E. The Electrochemistry of Noble Metal Electrodes in Aprotic Organic Solvents Containing Lithium Salts. *J. Electroanal. Chem. Interfacial Electrochem.* **1991**, *297*, 225–244.

(85) Kwabi, D. G.; Ortiz-Vitoriano, N.; Freunberger, S. A.; Chen, Y.; Imanishi, N.; Bruce, P. G.; Shao-Horn, Y. Materials Challenges in Rechargeable Lithium-Air Batteries. *MRS Bull.* **2014**, *39*, 443–452.

(86) Freunberger, S. A.; Chen, Y.; Peng, Z.; Griffin, J. M.; Hardwick, L. J.; Bardé, F.; Novák, P.; Bruce, P. G. Reactions in the Rechargeable Lithium–O_2 Battery with Alkyl Carbonate Electrolytes. *J. Am. Chem. Soc.* **2011**, *133*, 8040–8047.

(87) McCloskey, B. D.; Bethune, D. S.; Shelby, R. M.; Girishkumar, G.; Luntz, A. C. Solvents' Critical Role in Nonaqueous Lithium–Oxygen Battery Electrochemistry. *J. Phys. Chem. Lett.* **2011**, *2*, 1161–1166.

(88) Xu, W.; Viswanathan, V. V.; Wang, D.; Towne, S. A.; Xiao, J.; Nie, Z.; Hu, D.; Zhang, J.-G. Investigation on the Charging Process of Li_2O_2-Based Air Electrodes in Li–O_2 Batteries with Organic Carbonate Electrolytes. *J. Power Sources* **2011**, *196*, 3894–3899.

(89) Bryantsev, V. S.; Blanco, M. Computational Study of the Mechanisms of Superoxide-Induced Decomposition of Organic Carbonate-Based Electrolytes. *J. Phys. Chem. Lett.* **2011**, *2*, 379–383.

(90) Bryantsev, V. S. Predicting the Stability of Aprotic Solvents in Li-Air Batteries: pKa Calculations of Aliphatic C–H Acids in Dimethyl Sulfoxide. *Chem. Phys. Lett.* **2013**, *558*, 42–47.

(91) Khetan, A.; Pitsch, H.; Viswanathan, V. Solvent Degradation in Nonaqueous Li-O_2 Batteries: Oxidative Stability versus H-Abstraction. *J. Phys. Chem. Lett.* **2014**, *5*, 2419–2424.

(92) Melot, B. C.; Tarascon, J.-M. Design and Preparation of Materials for Advanced Electrochemical Storage. *Acc. Chem. Res.* **2013**, *46*, 1226–1238.

(93) Reynier, Y. F.; Yazami, R.; Fultz, B. Thermodynamics of Lithium Intercalation into Graphites and Disordered Carbons. *J. Electrochem. Soc.* **2004**, *151*, A422–A426.

(94) Wang, J.; Raistrick, I. D.; Huggins, R. A. Behavior of Some Binary Lithium Alloys as Negative Electrodes in Organic Solvent-Based Electrolytes. *J. Electrochem. Soc.* **1986**, *133*, 457–460.

(95) Weydanz, W. J.; Wohlfahrt-Mehrens, M.; Huggins, R. A. A Room Temperature Study of the Binary Lithium–silicon and the Ternary Lithium–chromium–silicon System for Use in Rechargeable Lithium Batteries. *J. Power Sources* **1999**, *81–82*, 237–242.

(96) Arai, H.; Okada, S.; Sakurai, Y.; Yamaki, J. Electrochemical and Structural Study of Li_2CuO_2, $LiCuO_2$ and $NaCuO_2$. *Solid State Ion.* **1998**, *106*, 45–53.

(97) Delmas, C.; Saadoune, I. Electrochemical and Physical Properties of the $Li_xNi_{1-y}Co_yO_2$ Phases. *Solid State Ion.* **1992**, *53–56, Part 1*, 370–375.

(98) de Picciotto, L. A.; Thackeray, M. M.; David, W. I. F.; Bruce, P. G.; Goodenough, J. B. Structural Characterization of Delithiated $LiVO_2$. *Mater. Res. Bull.* **1984**, *19*, 1497–1506.

(99) Whittingham, M. S. Electrical Energy Storage and Intercalation Chemistry. *Science* **1976**, *192*, 1126–1127.

(100) Imanishi, N.; Toyoda, M.; Takeda, Y.; Yamamoto, O. Study on Lithium Intercalation into MoS_2. *Solid State Ion.* **1992**, *58*, 333–338.

(101) Li, G.; Azuma, H.; Tohda, M. $LiMnPO_4$ as the Cathode for Lithium Batteries. *Electrochem. Solid-State Lett.* **2002**, *5*, A135–A137.

(102) Amine, K.; Yasuda, H.; Yamachi, M. Olivine $LiCoPO_4$ as 4.8 V Electrode Material for Lithium Batteries. *Electrochem. Solid-State Lett.* **2000**, *3*, 178–179.

(103) Zhou, F.; Cococcioni, M.; Kang, K.; Ceder, G. The Li Intercalation Potential of $LiMPO_4$ and $LiMSiO_4$ Olivines with M = Fe, Mn, Co, Ni. *Electrochem. Commun.* **2004**, *6*, 1144–1148.

(104)   Wolfenstine, J.; Allen, J. Ni^{3+}/Ni^{2+} Redox Potential in $LiNiPO_4$. *J. Power Sources* **2005**, *142*, 389–390.

(105)   Zhong, Q.; Bonakdarpour, A.; Zhang, M.; Gao, Y.; Dahn, J. R. Synthesis and Electrochemistry of $LiNi_xMn_{2-x}O_4$. *J. Electrochem. Soc.* **1997**, *144*, 205–213.

(106)   Lu, Y.-C.; Gasteiger, H. A.; Parent, M. C.; Chiloyan, V.; Shao-Horn, Y. The Influence of Catalysts on Discharge and Charge Voltages of Rechargeable Li–Oxygen Batteries. *Electrochem. Solid-State Lett.* **2010**, *13*, A69–A72.

(107)   Peled, E.; Yamin, H. Lithium/sulfur Organic Battery. *Prog. Batteries Sol. Cells* **1984**, *5*, 56–58.

(108)   Kim, Y.; Goodenough, J. B. Lithium Insertion into Transition-Metal Monosulfides: Tuning the Position of the Metal 4s Band. *J. Phys. Chem. C* **2008**, *112*, 15060–15064.

(109)   Goodenough, J. B.; Kim, Y. Locating Redox Couples in the Layered Sulfides with Application to $Cu[Cr_2]S_4$. *J. Solid State Chem.* **2009**, *182*, 2904–2911.

(110)   Ménétrier, M.; Carlier, D.; Blangero, M.; Delmas, C. On "Really" Stoichiometric $LiCoO_2$. *Electrochem. Solid-State Lett.* **2008**, *11*, A179–A182.

(111)   Croy, J. R.; Gallagher, K. G.; Balasubramanian, M.; Chen, Z.; Ren, Y.; Kim, D.; Kang, S.-H.; Dees, D. W.; Thackeray, M. M. Examining Hysteresis in Composite $_xLi_2MnO_3·(1-x)LiMO_2$ Cathode Structures. *J. Phys. Chem. C* **2013**, *117*, 6525–6536.

(112)   Thackeray, M. M.; Kang, S.-H.; Johnson, C. S.; Vaughey, J. T.; Benedek, R.; Hackney, S. A. Li_2MnO_3-Stabilized $LiMO_2$ (M = Mn, Ni, Co) Electrodes for Lithium-Ion Batteries. *J. Mater. Chem.* **2007**, *17*, 3112–3125.

(113)   Kim, J.-S.; Johnson, C. S.; Thackeray, M. M. Layered $xLiMO_2·(1-x)Li_2M'O_3$ Electrodes for Lithium Batteries: A Study of $0.95LiMn_{0.5}Ni_{0.5}O_2·0.05Li_2TiO_3$. *Electrochem. Commun.* **2002**, *4*, 205–209.

(114)   Koga, H.; Croguennec, L.; Mannessiez, P.; Ménétrier, M.; Weill, F.; Bourgeois, L.; Duttine, M.; Suard, E.; Delmas, C. $Li_{1.20}Mn_{0.54}Co_{0.13}Ni_{0.13}O_2$ with Different Particle Sizes as Attractive Positive Electrode Materials for Lithium-Ion Batteries: Insights into Their Structure. *J. Phys. Chem. C* **2012**, *116*, 13497–13506.

(115)   Ates, M. N.; Mukerjee, S.; Abraham, K. M. A Search for the Optimum Lithium Rich Layered Metal Oxide Cathode Material for Li-Ion Batteries. *J. Electrochem. Soc.* **2015**, *162*, A1236–A1245.

(116)   Robertson, A. D.; Bruce, P. G. Mechanism of Electrochemical Activity in Li_2MnO_3. *Chem. Mater.* **2003**, *15*, 1984–1992.

(117)   Sathiya, M.; Abakumov, A. M.; Foix, D.; Rousse, G.; Ramesha, K.; Saubanère, M.; Doublet, M. L.; Vezin, H.; Laisa, C. P.; Prakash, A. S.; et al. Origin of Voltage Decay in High-Capacity Layered Oxide Electrodes. *Nat. Mater.* **2015**, *14*, 230–238.

(118)   Tarascon, J. M.; Vaughan, G.; Chabre, Y.; Seguin, L.; Anne, M.; Strobel, P.; Amatucci, G. In Situ Structural and Electrochemical Study of $Ni_{1-x}Co_xO_2$ Metastable Oxides Prepared by Soft Chemistry. *J. Solid State Chem.* **1999**, *147*, 410–420.

(119)   Rivadulla, F.; Zhou, J.-S.; Goodenough, J. B. Chemical, Structural, and Transport Properties of $Na_{1-x}CoO_2$. *Phys. Rev. B* **2003**, *68*, 075108.

(120)   Chebiam, R. V.; Kannan, A. M.; Prado, F.; Manthiram, A. Comparison of the Chemical Stability of the High Energy Density Cathodes of Lithium-Ion Batteries. *Electrochem. Commun.* **2001**, *3*, 624–627.

(121) Venkatraman, S.; Shin, Y.; Manthiram, A. Phase Relationships and Structural and Chemical Stabilities of Charged $Li_{1-x}CoO_{2-\delta}$ and $Li_{1-x}Ni_{0.85}Co_{0.15}O_{2-\delta}$ Cathodes. *Electrochem. Solid-State Lett.* **2003**, *6*, A9–A12.

(122) Johnson, L.; Li, C.; Liu, Z.; Chen, Y.; Freunberger, S. A.; Ashok, P. C.; Praveen, B. B.; Dholakia, K.; Tarascon, J.-M.; Bruce, P. G. The Role of LiO_2 Solubility in O_2 Reduction in Aprotic Solvents and Its Consequences for $Li-O_2$ Batteries. *Nat. Chem.* **2014**, *6*, 1091–1099.

(123) Vollmer, J. M.; Curtiss, L. A.; Vissers, D. R.; Amine, K. Reduction Mechanisms of Ethylene, Propylene, and Vinylethylene Carbonates A Quantum Chemical Study. *J. Electrochem. Soc.* **2004**, *151*, A178–A183.

(124) Borodin, O.; Jow, T. R. Quantum Chemistry Studies of the Oxidative Stability of Carbonate, Sulfone and Sulfonate-Based Electrolytes Doped with BF_4^-, PF_6^- Anions. *ECS Trans.* **2011**, *33*, 77–84.

(125) Malmgren, S.; Ciosek, K.; Lindblad, R.; Plogmaker, S.; Kühn, J.; Rensmo, H.; Edström, K.; Hahlin, M. Consequences of Air Exposure on the Lithiated Graphite SEI. *Electrochim. Acta* **2013**, *105*, 83–91.

(126) Jiang, J.; Dahn, J. R. Effects of Solvents and Salts on the Thermal Stability of LiC_6. *Electrochim. Acta* **2004**, *49*, 4599–4604.

(127) Chattopadhyay, S.; Lipson, A. L.; Karmel, H. J.; Emery, J. D.; Fister, T. T.; Fenter, P. A.; Hersam, M. C.; Bedzyk, M. J. In Situ X-Ray Study of the Solid Electrolyte Interphase (SEI) Formation on Graphene as a Model Li-Ion Battery Anode. *Chem. Mater.* **2012**, *24*, 3038–3043.

(128) Zaban, A.; Zinigrad, E.; Aurbach, D. Impedance Spectroscopy of Li Electrodes. 4. A General Simple Model of the Li–Solution Interphase in Polar Aprotic Systems. *J. Phys. Chem.* **1996**, *100*, 3089–3101.

(129) Bar-Tow, D.; Peled, E.; Burstein, L. A Study of Highly Oriented Pyrolytic Graphite as a Model for the Graphite Anode in Li-Ion Batteries. *J. Electrochem. Soc.* **1999**, *146*, 824–832.

(130) Johansson, P.; Jacobsson, P. Rational Design of Electrolyte Components by Ab Initio Calculations. *J. Power Sources* **2006**, *153*, 336–344.

(131) Endo, E.; Ata, M.; Tanaka, K.; Sekai, K. Electron Spin Resonance Study of the Electrochemical Reduction of Electrolyte Solutions for Lithium Secondary Batteries. *J. Electrochem. Soc.* **1998**, *145*, 3757–3764.

(132) Qiao, R.; Lucas, I. T.; Karim, A.; Syzdek, J.; Liu, X.; Chen, W.; Persson, K.; Kostecki, R.; Yang, W. Distinct Solid-Electrolyte-Interphases on Sn (100) and (001) Electrodes Studied by Soft X-Ray Spectroscopy. *Adv. Mater. Interfaces* **2014**, *1*, 1300115.

(133) Owejan, J. E.; Owejan, J. P.; DeCaluwe, S. C.; Dura, J. A. Solid Electrolyte Interphase in Li-Ion Batteries: Evolving Structures Measured In Situ by Neutron Reflectometry. *Chem. Mater.* **2012**, *24*, 2133–2140.

(134) Veith, G. M.; Baggetto, L.; Sacci, R. L.; Unocic, R. R.; Tenhaeff, W. E.; Browning, J. F. Direct Measurement of the Chemical Reactivity of Silicon Electrodes with $LiPF_6$-Based Battery Electrolytes. *Chem. Commun.* **2014**, *50*, 3081–3084.

(135) Peled, E. Film Forming Reaction at the Lithium/electrolyte Interface. *J. Power Sources* **1983**, *9*, 253–266.

(136) Gabano, J.-P. *Lithium Batteries*; Academic Press: London, New York, 1983.

(137) Aurbach, D.; Daroux, M. L.; Faguy, P. W.; Yeager, E. Identification of Surface Films Formed on Lithium in Propylene Carbonate Solutions. *J. Electrochem. Soc.* **1987**, *134*, 1611–1620.

(138) Dey, A. N. Lithium Anode Film and Organic and Inorganic Electrolyte Batteries. *Thin Solid Films* **1977**, *43*, 131–171.

(139) Besenhard, J. O.; Winter, M.; Yang, J.; Biberacher, W. Filming Mechanism of Lithium-Carbon Anodes in Organic and Inorganic Electrolytes. *J. Power Sources* **1995**, *54*, 228–231.

(140) Aurbach, D.; Zaban, A.; Gofer, Y.; Ely, Y. E.; Weissman, I.; Chusid, O.; Abramson, O. Recent Studies of the Lithium-Liquid Electrolyte Interface Electrochemical, Morphological and Spectral Studies of a Few Important Systems. *J. Power Sources* **1995**, *54*, 76–84.

(141) Chusid (Youngman), O.; Ein Ely, E.; Aurbach, D.; Babai, M.; Carmeli, Y. Electrochemical and Spectroscopic Studies of Carbon Electrodes in Lithium Battery Electrolyte Systems. *J. Power Sources* **1993**, *43*, 47–64.

(142) Aurbach, D.; Gofer, Y.; Ben-Zion, M.; Aped, P. The Behaviour of Lithium Electrodes in Propylene and Ethylene Carbonate: The Major Factors That Influence Li Cycling Efficiency. *J. Electroanal. Chem.* **1992**, *339*, 451–471.

(143) Zhuang, G. V.; Xu, K.; Yang, H.; Jow, T. R.; Ross, P. N. Lithium Ethylene Dicarbonate Identified as the Primary Product of Chemical and Electrochemical Reduction of EC in 1.2 M $LiPF_6$/EC:EMC Electrolyte. *J. Phys. Chem. B* **2005**, *109*, 17567–17573.

(144) Cohen, Y. S.; Cohen, Y.; Aurbach, D. Micromorphological Studies of Lithium Electrodes in Alkyl Carbonate Solutions Using in Situ Atomic Force Microscopy. *J. Phys. Chem. B* **2000**, *104*, 12282–12291.

(145) Gofer, Y.; Ben-Zion, M.; Aurbach, D. Solutions of $LiAsF_6$ in 1,3-Dioxolane for Secondary Lithium Batteries. *J. Power Sources* **1992**, *39*, 163–178.

(146) Qian, J.; Henderson, W. A.; Xu, W.; Bhattacharya, P.; Engelhard, M.; Borodin, O.; Zhang J-G. High rate and stable cycling of lithium metal anode. *Nat. Comm.* **2015**, *6*, 6362.

(147) Suo, L.; Hu, Y-S.; Li, H.; Armand, M.; Chen, L. A new class of Solvent-in-Salt electrolyte for high-energy rechargeable metallic lithium batteries. *Nat. Comm.* **2013**, *4*, 1481.

(148) Yamada, Y.; Furukama, K.; Sodeyama, K.; Kikuchi, K.; Yaegashi, M.; Tateyama, Y.; Yamada, A. Unusual Stability of Acetonitrile-Based Superconcentrated Electrolytes for Fast-Charging Lithium-Ion Batteries. *J. Am. Chem. Soc.* **2014**, *136*, 5039-5046.

(149) Peled, E.; Towa, D. B.; Merson, A.; Burstein, L. Microphase Structure of SEI on HOPG. *J. New Mater. Electrochem. Syst.* **2000**, *3*, 319–326.

(150) Aurbach, D.; Ein-Eli, Y.; Markovsky, B.; Zaban, A.; Luski, S.; Carmeli, Y.; Yamin, H. The Study of Electrolyte Solutions Based on Ethylene and Diethyl Carbonates for Rechargeable Li Batteries II. Graphite Electrodes. *J. Electrochem. Soc.* **1995**, *142*, 2882–2890.

(151) Aurbach, D.; Levi, M. D.; Levi, E.; Schechter, A. Failure and Stabilization Mechanisms of Graphite Electrodes. *J. Phys. Chem. B* **1997**, *101*, 2195–2206.

(152) Aurbach, D.; Markovsky, B.; Weissman, I.; Levi, E.; Ein-Eli, Y. On the Correlation between Surface Chemistry and Performance of Graphite Negative Electrodes for Li Ion Batteries. *Electrochim. Acta* **1999**, *45*, 67–86.

(153) Aurbach, D.; Zaban, A.; Ein-Eli, Y.; Weissman, I.; Chusid, O.; Markovsky, B.; Levi, M.; Levi, E.; Schechter, A.; Granot, E. Recent Studies on the Correlation between Surface Chemistry, Morphology, Three-Dimensional Structures and Performance of Li and Li-C Intercalation Anodes in Several Important Electrolyte Systems. *J. Power Sources* **1997**, *68*, 91–98.

(154) Aurbach, D.; Ein-Eli, Y.; Chusid (Youngman), O.; Carmeli, Y.; Babai, M.; Yamin, H. The Correlation Between the Surface Chemistry and the Performance of Li-Carbon Intercalation Anodes for Rechargeable "Rocking-Chair" Type Batteries. *J. Electrochem. Soc.* **1994**, *141*, 603–611.

(155) Ein-Eli, Y.; Markovsky, B.; Aurbach, D.; Carmeli, Y.; Yamin, H.; Luski, S. The Dependence of the Performance of Li-C Intercalation Anodes for Li-Ion Secondary Batteries on the Electrolyte Solution Composition. *Electrochim. Acta* **1994**, *39*, 2559–2569.

(156) Jeong, S.-K.; Inaba, M.; Iriyama, Y.; Abe, T.; Ogumi, Z. AFM Study of Surface Film Formation on a Composite Graphite Electrode in Lithium-Ion Batteries. *J. Power Sources* **2003**, *119–121*, 555–560.

(157) Augustsson, A.; Herstedt, M.; Guo, J.-H.; Edström, K.; Zhuang, G. V.; P. N. Ross, J.; Rubensson, J.-E.; Nordgren, J. Solid Electrolyte Interphase on Graphite Li-Ion Battery Anodes Studied by Soft X-Ray Spectroscopy. *Phys. Chem. Chem. Phys.* **2004**, *6*, 4185–4189.

(158) Leifer, N.; Smart, M. C.; Prakash, G. K. S.; Gonzalez, L.; Sanchez, L.; Smith, K. A.; Bhalla, P.; Grey, C. P.; Greenbaum, S. G. ^{13}C Solid State NMR Suggests Unusual Breakdown Products in SEI Formation on Lithium Ion Electrodes. *J. Electrochem. Soc.* **2011**, *158*, A471–A480.

(159) Lu, P.; Li, C.; Schneider, E. W.; Harris, S. J. Chemistry, Impedance, and Morphology Evolution in Solid Electrolyte Interphase Films during Formation in Lithium Ion Batteries. *J. Phys. Chem. C* **2014**, *118*, 896-903.

(160) Funabiki, A.; Inaba, M.; Ogumi, Z. A.c. Impedance Analysis of Electrochemical Lithium Intercalation into Highly Oriented Pyrolytic Graphite. *J. Power Sources* **1997**, *68*, 227–231.

(161) Wagner, M. R.; Albering, J. H.; Moeller, K.-C.; Besenhard, J. O.; Winter, M. XRD Evidence for the Electrochemical Formation of in PC-Based Electrolytes. *Electrochem. Commun.* **2005**, *7*, 947–952.

(162) Xu, K.; Lam, Y.; Zhang, S. S.; Jow, T. R.; Curtis, T. B. Solvation Sheath of Li$^+$ in Nonaqueous Electrolytes and Its Implication of Graphite/Electrolyte Interface Chemistry. *J. Phys. Chem. C* **2007**, *111*, 7411–7421.

(163) Shkrob, I. A.; Zhu, Y.; Marin, T. W.; Abraham, D. Reduction of Carbonate Electrolytes and the Formation of Solid-Electrolyte Interface (SEI) in Lithium-Ion Batteries. 1. Spectroscopic Observations of Radical Intermediates Generated in One-Electron Reduction of Carbonates. *J. Phys. Chem. C* **2013**, *117*, 19255–19269.

(164) Shkrob, I. A.; Zhu, Y.; Marin, T. W.; Abraham, D. Reduction of Carbonate Electrolytes and the Formation of Solid-Electrolyte Interface (SEI) in Lithium-Ion Batteries. 2.

Radiolytically Induced Polymerization of Ethylene Carbonate. *J. Phys. Chem. C* **2013**, *117*, 19270–19279.

(165) Banks, C. E.; Davies, T. J.; Wildgoose, G. G.; Compton, R. G. Electrocatalysis at Graphite and Carbon Nanotube Modified Electrodes: Edge-Plane Sites and Tube Ends Are the Reactive Sites. *Chem. Commun.* **2005**, *7*, 829–841.

(166) Kneten, K. R.; McCreery, R. L. Effects of Redox System Structure on Electron-Transfer Kinetics at Ordered Graphite and Glassy Carbon Electrodes. *Anal. Chem.* **1992**, *64*, 2518–2524.

(167) McCreery, R. L. Advanced Carbon Electrode Materials for Molecular Electrochemistry. *Chem. Rev.* **2008**, *108*, 2646–2687.

(168) Bedrov, D.; Smith, G. D.; van Duin, A. C. T. Reactions of Singly-Reduced Ethylene Carbonate in Lithium Battery Electrolytes: A Molecular Dynamics Simulation Study Using the ReaxFF. *J. Phys. Chem. A* **2012**, *116*, 2978–2985.

(169) Dey, A. N.; Sullivan, B. P. The Electrochemical Decomposition of Propylene Carbonate on Graphite. *J. Electrochem. Soc.* **1970**, *117*, 222–224.

(170) Xu, K.; Zhuang, G. V.; Allen, J. L.; Lee, U.; Zhang, S. S.; Ross, Philip N.; Jow, T. R. Syntheses and Characterization of Lithium Alkyl Mono- and Dicarbonates as Components of Surface Films in Li-Ion Batteries. *J. Phys. Chem. B* **2006**, *110*, 7708–7719.

(171) Ein-Eli, Y.; McDevitt, S. F.; Aurbach, D.; Markovsky, B.; Schechter, A. Methyl Propyl Carbonate: A Promising Single Solvent for Li-ion Battery Electrolytes. *J. Electrochem. Soc.* **1997**, *144*, L180–L184.

(172) Sloop, S. E.; Pugh, J. K.; Wang, S.; Kerr, J. B.; Kinoshita, K. Chemical Reactivity of PF_5 and $LiPF_6$ in Ethylene Carbonate/Dimethyl Carbonate Solutions. *Electrochem. Solid-State Lett.* **2001**, *4*, A42–A44.

(173) Andersson, A. M.; Edström, K. Chemical Composition and Morphology of the Elevated Temperature SEI on Graphite. *J. Electrochem. Soc.* **2001**, *148*, A1100–A1109.

(174) Choi, N.-S.; Yew, K. H.; Lee, K. Y.; Sung, M.; Kim, H.; Kim, S.-S. Effect of Fluoroethylene Carbonate Additive on Interfacial Properties of Silicon Thin-Film Electrode. *J. Power Sources* **2006**, *161*, 1254–1259.

(175) Chan, C. K.; Ruffo, R.; Hong, S. S.; Cui, Y. Surface Chemistry and Morphology of the Solid Electrolyte Interphase on Silicon Nanowire Lithium-Ion Battery Anodes. *J. Power Sources* **2009**, *189*, 1132–1140.

(176) Yen, Y.-C.; Chao, S.-C.; Wu, H.-C.; Wu, N.-L. Study on Solid-Electrolyte-Interphase of Si and C-Coated Si Electrodes in Lithium Cells. *J. Electrochem. Soc.* **2009**, *156*, A95–A102.

(177) Philippe, B.; Dedryvère, R.; Allouche, J.; Lindgren, F.; Gorgoi, M.; Rensmo, H.; Gonbeau, D.; Edström, K. Nanosilicon Electrodes for Lithium-Ion Batteries: Interfacial Mechanisms Studied by Hard and Soft X-Ray Photoelectron Spectroscopy. *Chem. Mater.* **2012**, *24*, 1107–1115.

(178) Xu, W.; Vegunta, S. S. S.; Flake, J. C. Surface-Modified Silicon Nanowire Anodes for Lithium-Ion Batteries. *J. Power Sources* **2011**, *196*, 8583–8589.

(179) Song, S.-W.; Baek, S.-W. Surface Layer Formation on Sn Anode: ATR FTIR Spectroscopic Characterization. *Electrochim. Acta* **2009**, *54*, 1312–1318.

(180) Li, J.-T.; Chen, S.-R.; Fan, X.-Y.; Huang, L.; Sun, S.-G. Studies of the Interfacial Properties of an Electroplated Sn Thin Film Electrode/Electrolyte Using in Situ MFTIRS and EQCM. *Langmuir* **2007**, *23*, 13174–13180.

(181) Park, S.; Ryu, J. H.; Oh, S. M. Passivating Ability of Surface Film Derived from Vinylene Carbonate on Tin Negative Electrode. *J. Electrochem. Soc*. **2011**, *158*, A498–A503.

(182) Pereira-Nabais, C.; Światowska, J.; Chagnes, A.; Gohier, A.; Zanna, S.; Seyeux, A.; Tran-Van, P.; Cojocaru, C.-S.; Cassir, M.; Marcus, P. Insight into the Solid Electrolyte Interphase on Si Nanowires in Lithium-Ion Battery: Chemical and Morphological Modifications upon Cycling. *J. Phys. Chem. C* **2014**, *118*, 2919–2928.

(183) Philippe, B.; Dedryvère, R.; Gorgoi, M.; Rensmo, H.; Gonbeau, D.; Edström, K. Role of the $LiPF_6$ Salt for the Long-Term Stability of Silicon Electrodes in Li-Ion Batteries – A Photoelectron Spectroscopy Study. *Chem. Mater*. **2013**, *25*, 394–404.

(184) Liu, N.; Lu, Z.; Zhao, J.; McDowell, M. T.; Lee, H.-W.; Zhao, W.; Cui, Y. A Pomegranate-Inspired Nanoscale Design for Large-Volume-Change Lithium Battery Anodes. *Nat. Nanotechnol*. **2014**, *9*, 187–192.

(185) Lucas, I. T.; Syzdek, J.; Kostecki, R. Interfacial Processes at Single-Crystal β-Sn Electrodes in Organic Carbonate Electrolytes. *Electrochem. Commun*. **2011**, *13*, 1271–1275.

(186) Jarry A., Knitsch R.; Lux S. F., Kostecki R.. SEI Formation on Single Crystal Si Electrodes in Organic Carbonate Electrolytes; Abstract, 225th ECS Meeting , Orlando, 2014.

(187) Vogl, U. S.; Lux, S. F.; Crumlin, E. J.; Liu, Z.; Terborg, L.; Winter, M.; Kostecki, R. The Mechanism of SEI Formation on a Single Crystal Si(100) Electrode. *J. Electrochem. Soc*. **2015**, *162*, A603–A607.

(188) Kaghazchi, P. Phase-Sensitivity of Li Intercalation into Sn. *J. Phys. Condens. Matter* **2013**, *25*, 382204.

(189) Aurbach, D.; Markovsky, B.; Rodkin, A.; Levi, E.; Cohen, Y.; Kim, H.-J.; Schmidt, M. On the Capacity Fading of $LiCoO_2$ Intercalation Electrodes:: The Effect of Cycling, Storage, Temperature, and Surface Film Forming Additives. *Electrochim. Acta* **2002**, *47*, 4291–4306.

(190) Dedryvère, R.; Foix, D.; Franger, S.; Patoux, S.; Daniel, L.; Gonbeau, D. Electrode/Electrolyte Interface Reactivity in High-Voltage Spinel $LiMn_{1.6}Ni_{0.4}O_4/Li_4Ti_5O_{12}$ Lithium-Ion Battery. *J. Phys. Chem. C* **2010**, *114*, 10999–11008.

(191) Kanamura, K.; Toriyama, S.; Shiraishi, S.; Ohashi, M.; Takehara, Z. Studies on Electrochemical Oxidation of Non-Aqueous Electrolyte on the $LiCoO_2$ Thin Film Electrode. *J. Electroanal. Chem*. **1996**, *419*, 77–84.

(192) Aurbach, D.; Levi, M. D.; Levi, E.; Teller, H.; Markovsky, B.; Salitra, G.; Heider, U.; Heider, L. Common Electroanalytical Behavior of Li Intercalation Processes into Graphite and Transition Metal Oxides. *J. Electrochem. Soc*. **1998**, *145*, 3024–3034.

(193) Takamatsu, D.; Koyama, Y.; Orikasa, Y.; Mori, S.; Nakatsutsumi, T.; Hirano, T.; Tanida, H.; Arai, H.; Uchimoto, Y.; Ogumi, Z. First In Situ Observation of the $LiCoO_2$ Electrode/Electrolyte Interface by Total-Reflection X-Ray Absorption Spectroscopy. *Angew. Chem. Int. Ed*. **2012**, *51*, 11597–11601.

(194) Lin, F.; Markus, I. M.; Nordlund, D.; Weng, T-C.; Asta, M. D.; Xin, H. L.; Doeff, M. M. Surface reconstruction and chemical evolution of stoichiometric layered cathode materials for lithium-ion batteries. *Nat. Comm.* **2014**, *5*, DOI: 10.1038/ncomms4529.

(195) Jung, S-K.; Gwon, H.; Hong, J.; Park, K-Y.; Seo, D-H.; Kim, H.; Hyun, J.; Yang, W.; Kang, K. Understanding the Degradation Mechanisms of $LiNi_{0.5}Co_{0.2}Mn_{0.3}O_2$ Cathode Material in Lithium Ion Batteries. *Adv. Energy Mater.* **2014**, *4*, 1300787.

(196) Hwang, S.; Chang, W.; Kim, S. M.; Su, D.; Kim, D. H.; Lee, J. Y.; Chung, K. Y.; Stach, E. A. Investigation of Changes in the Surface Structure of $Li_xNi_{0.8}Co_{0.15}Al_{0.05}O_2$ Cathode Materials Induced by the Initial Charge. *Chem. Mater.* **2014**, *26*, 1084–92.

(197) Boulineau, A.; Simonin, S.; Colin, J-F.; Canévet, E.; Daniel, L.; Patoux, S. Evolutions of $Li_{1.2}Mn_{0.61}Ni_{0.18}Mg_{0.01}O_2$ during the Initial Charge/Discharge Cycle Studied by Advanced Electron Microscopy. *Chem. Mater.* **2012**, *24*, 3558–66.

(198) Aurbach, D.; Weissman, I.; Schechter, A.; Cohen, H. X-Ray Photoelectron Spectroscopy Studies of Lithium Surfaces Prepared in Several Important Electrolyte Solutions. A Comparison with Previous Studies by Fourier Transform Infrared Spectroscopy. *Langmuir* **1996**, *12*, 3991–4007.

(199) Aurbach, D.; Zaban, A.; Schechter, A.; Ein-Eli, Y.; Zinigrad, E.; Markovsky, B. The Study of Electrolyte Solutions Based on Ethylene and Diethyl Carbonates for Rechargeable Li Batteries I . Li Metal Anodes. *J. Electrochem. Soc.* **1995**, *142*, 2873–2882.

(200) Markevich, E.; Salitra, G.; Aurbach, D. Influence of the PVdF Binder on the Stability of $LiCoO_2$ Electrodes. *Electrochem. Commun.* **2005**, *7*, 1298–1304.

(201) Chang, H.-H.; Chang, C.-C.; Su, C.-Y.; Wu, H.-C.; Yang, M.-H.; Wu, N.-L. Effects of TiO_2 Coating on High-Temperature Cycle Performance of $LiFePO_4$-Based Lithium-Ion Batteries. *J. Power Sources* **2008**, *185*, 466–472.

(202) Chang, H.-H.; Wu, H.-C.; Wu, N.-L. Enhanced High-Temperature Cycle Performance of $LiFePO_4$/carbon Batteries by an Ion-Sieving Metal Coating on Negative Electrode. *Electrochem. Commun.* **2008**, *10*, 1823–1826.

(203) Cho, J.; Kim, Y. J.; Park, B. Novel $LiCoO_2$ Cathode Material with Al_2O_3 Coating for a Li Ion Cell. *Chem. Mater.* **2000**, *12*, 3788–3791.

(204) Oh, S.; Lee, J. K.; Byun, D.; Cho, W. I.; Won Cho, B. Effect of Al_2O_3 Coating on Electrochemical Performance of $LiCoO_2$ as Cathode Materials for Secondary Lithium Batteries. *J. Power Sources* **2004**, *132*, 249–255.

(205) Verdier, S.; Ouatani, L. El; Dedryvere, R.; Bonhomme, F.; Biensan, P.; Gonbeau, D. XPS Study on Al_2O_3- and $AlPO_4$-Coated $LiCoO_2$ Cathode Material for High-Capacity Li Ion Batteries. *J. Electrochem. Soc.* **2007**, *154*, A1088–A1099.

(206) Levi, M. D.; Salitra, G.; Markovsky, B.; Teller, H.; Aurbach, D.; Heider, U.; Heider, L. Solid-State Electrochemical Kinetics of Li-Ion Intercalation into $Li_{1-x}CoO_2$: Simultaneous Application of Electroanalytical Techniques SSCV, PITT, and EIS. *J. Electrochem. Soc.* **1999**, *146*, 1279–1289.

(207) Aurbach, D.; Markovsky, B.; Salitra, G.; Markevich, E.; Talyossef, Y.; Koltypin, M.; Nazar, L.; Ellis, B.; Kovacheva, D. Review on Electrode-Electrolyte Solution Interactions, Related to Cathode Materials for Li-Ion Batteries. *J. Power Sources* **2007**, *165*, 491–499.

(208) Di Valentin, C.; Locati, C.; Pacchioni, G. Probing the Basicity of Regular and Defect Sites of Alkaline Earth Metal Oxide Surfaces by BF_3 Adsorption: A Theoretical Analysis. *ChemPhysChem* **2004**, *5*, 642–651.

(209) Ensling, D.; Cherkashinin, G.; Schmid, S.; Bhuvaneswari, S.; Thissen, A.; Jaegermann, W. Nonrigid Band Behavior of the Electronic Structure of $LiCoO_2$ Thin Film during Electrochemical Li Deintercalation. *Chem. Mater.* **2014**, *26*, 3948–3956.

(210) Wang, H.; Rus, E.; Sakuraba, T.; Kikuchi, J.; Kiya, Y.; Abruña, H. D. CO_2 and O_2 Evolution at High Voltage Cathode Materials of Li-Ion Batteries: A Differential Electrochemical Mass Spectrometry Study. *Anal. Chem.* **2014**, *86*, 6197–6201.

(211) Hong, J.; Lim, H.-D.; Lee, M.; Kim, S.-W.; Kim, H.; Oh, S.-T.; Chung, G.-C.; Kang, K. Critical Role of Oxygen Evolved from Layered Li–Excess Metal Oxides in Lithium Rechargeable Batteries. *Chem. Mater.* **2012**, *24*, 2692–2697.

(212) Mantia, F. L.; Rosciano, F.; Tran, N.; Novák, P. Direct Evidence of Oxygen Evolution from $Li_{1+x}(Ni_{1/3}Mn_{1/3}Co_{1/3})_{1-x}O_2$ at High Potentials. *J. Appl. Electrochem.* **2008**, *38*, 893–896.

(213) Sathiya, M.; Leriche, J.-B.; Salager, E.; Gourier, D.; Tarascon, J.-M.; Vezin, H. Electron Paramagnetic Resonance Imaging for Real-Time Monitoring of Li-Ion Batteries. *Nat. Commun.* **2015**, *6*, 6276.

(214) Koga, H.; Croguennec, L.; Ménétrier, M.; Mannessiez, P.; Weill, F.; Delmas, C.; Belin, S. Operando X-Ray Absorption Study of the Redox Processes Involved upon Cycling of the Li-Rich Layered Oxide $Li_{1.20}Mn_{0.54}Co0_{.13}Ni_{0.13}O_2$ in Li Ion Batteries. *J. Phys. Chem. C* **2014**, *118*, 5700–5709.

(215) Koga, H.; Croguennec, L.; Ménétrier, M.; Douhil, K.; Belin, S.; Bourgeois, L.; Suard, E.; Weill, F.; Delmas, C. Reversible Oxygen Participation to the Redox Processes Revealed for $Li1_{.20}Mn_{0.54}Co_{0.13}Ni_{0.13}O_2$. *J. Electrochem. Soc.* **2013**, *160*, A786–A792.

(216) Thackeray, M. M.; Johnson, C. S.; Vaughey, J. T.; Li, N.; Hackney, S. A. Advances in Manganese-Oxide "composite" Electrodes for Lithium-Ion Batteries. *J. Mater. Chem.* **2005**, *15*, 2257–2267.

(217) Yu, D. Y. W.; Yanagida, K.; Kato, Y.; Nakamura, H. Electrochemical Activities in Li_2MnO_3. *J. Electrochem. Soc.* **2009**, *156*, A417–A424.

(218) Armstrong, A. R.; Robertson, A. D.; Bruce, P. G. Overcharging Manganese Oxides: Extracting Lithium beyond Mn^{4+}. *J. Power Sources* **2005**, *146*, 275–280.

(219) Guilmard, M.; Croguennec, L.; Delmas, C. Thermal Stability of Lithium Nickel Oxide Derivatives. Part II: $Li_xNi_{0.70}Co_{0.15}Al_{0.15}O_2$ and $Li_xNi_{0.90}Mn0_{.10}O_2$ (x = 0.50 and 0.30). Comparison with $Li_xNi_{1.02}O_2$ and $Li_xNi_{0.89}Al_{0.16}O_2$. *Chem. Mater.* **2003**, *15*, 4484–4493.

(220) Yabuuchi, N.; Kim, Y.-T.; Li, H. H.; Shao-Horn, Y. Thermal Instability of Cycled $Li_xNi_{0.5}Mn_{0.5}O_2$ Electrodes: An in Situ Synchrotron X-Ray Powder Diffraction Study. *Chem. Mater.* **2008**, *20*, 4936–4951.

(221) Dupré, N.; Cuisinier, M.; Legall, E.; War, D.; Guyomard, D. Contribution of the oxygen extracted from overlithiated layered oxides at high potential to the formation of the interphase. *J. Power Sources* **2015**, *299*, 231-240.

(222) Bryantsev, V. S.; Giordani, V.; Walker, W.; Blanco, M.; Zecevic, S.; Sasaki, K.; Uddin, J.; Addison, D.; Chase, G. V. Predicting Solvent Stability in Aprotic Electrolyte Li–Air Batteries: Nucleophilic Substitution by the Superoxide Anion Radical ($O2\bullet-$). J. Phys. Chem. A 2011, 115, 12399–12409.

(223) Bryantsev, V. S.; Faglioni, F. Predicting Autoxidation Stability of Ether- and Amide-Based Electrolyte Solvents for Li–Air Batteries. *J. Phys. Chem. A* **2012**, *116*, 7128–7138.

(224) Fransson, L.; Eriksson, T.; Edström, K.; Gustafsson, T.; Thomas, J. O. Influence of Carbon Black and Binder on Li-Ion Batteries. *J. Power Sources* **2001**, *101*, 1–9.

(225) Lux, S. F.; Pollak, E.; Boesenberg, U.; Richardson, T.; Kostecki, R. Electrochemical Reactivity of Pyrolytic Carbon Film Electrodes in Organic Carbonate Electrolytes. *Electrochem. Commun.* **2014**, *46*, 5–8.

(226) Pasquier, A. D.; Disma, F.; Bowmer, T.; Gozdz, A. S.; Amatucci, G.; Tarascon, J.-M. Differential Scanning Calorimetry Study of the Reactivity of Carbon Anodes in Plastic Li-Ion Batteries. *J. Electrochem. Soc.* **1998**, *145*, 472–477.

(227) Maibach, J.; Xu, C.; Eriksson, S. K.; Åhlund, J.; Gustafsson, T.; Siegbahn, H.; Rensmo, H.; Edström, K.; Hahlin, M. A High Pressure X-Ray Photoelectron Spectroscopy Experimental Method for Characterization of Solid-Liquid Interfaces Demonstrated with a Li-Ion Battery System. *Rev. Sci. Instrum.* **2015**, 86, 044101.

Quotes to highlight in paper:

1) Recent advances in high-capacity positive materials, which can generate highly reactive oxygen species, highlight the need to study EEI layers on their surfaces.

2) There is still limited understanding on what EEI layers consist of, by what mechanisms they are formed and how they influence EEI properties and battery performance.

3) Although the well-known mosaic model of the SEI on lithium and graphite is well accepted in the community, it has not been fully experimentally established and enough challenged

4) The development of synchrotron and *in situ* techniques should help find the missing pieces of the SEI puzzle

5) Further studies are needed to understand the effect of oxygen products such as O2 gas, superoxide or peroxo-like species on the EEI layers

6) there is a need for study of model electrode surfaces such as oxide pellets and thin films, which allow for investigating the reactivity of the electrolyte with the active material surface alone